AMERICAN SOCIETY FOR MICROBIOLOGY | Journal of Virology®

VIRUS-CELL INTERACTIONS

Identification of the RNA Pseudoknot within the 3′ End of the Porcine Reproductive and Respiratory Syndrome Virus Genome as a Pathogen-Associated Molecular Pattern To Activate Antiviral Signaling via RIG-I and Toll-Like Receptor 3

Sha Xie,[a,b] Xin-xin Chen,[b] Songlin Qiao,[b] Rui Li,[b] Yangang Sun,[b,c] Shuangfei Xia,[d] Lin-Jian Wang,[b] Xuegang Luo,[a,b] Ruiguang Deng,[b] En-Min Zhou,[a] Gai-Ping Zhang[a,b,d]

[a]College of Veterinary Medicine, Northwest A&F University, Yangling, People's Republic of China

[b]Key Laboratory of Animal Immunology of the Ministry of Agriculture, Henan Provincial Key Laboratory of Animal Immunology, Henan Academy of Agricultural Sciences, Zhengzhou, China

[c]College of Veterinary Medicine, Jilin University, Changchun, China

[d]College of Animal Science and Veterinary Medicine, Henan Agricultural University, Zhengzhou, People's Republic of China

ABSTRACT Once infected by viruses, cells can detect pathogen-associated molecular patterns (PAMPs) on viral nucleic acid by host pattern recognition receptors (PRRs) to initiate the antiviral response. Porcine reproductive and respiratory syndrome virus (PRRSV) is the causative agent of porcine reproductive and respiratory syndrome (PRRS), characterized by reproductive failure in sows and respiratory diseases in pigs of different ages. To date, the sensing mechanism of PRRSV has not been elucidated. Here, we reported that the pseudoknot region residing in the 3′ untranslated regions (UTR) of the PRRSV genome, which has been proposed to regulate RNA synthesis and virus replication, was sensed as nonself by retinoic acid-inducible gene I (RIG-I) and Toll-like receptor 3 (TLR3) and strongly induced type I interferons (IFNs) and interferon-stimulated genes (ISGs) in porcine alveolar macrophages (PAMs). The interaction between the two stem-loops inside the pseudoknot structure was sufficient for IFN induction, since disruption of the pseudoknot interaction powerfully dampened the IFN induction. Furthermore, transfection of the 3′ UTR pseudoknot transcripts in PAMs inhibited PRRSV replication *in vitro*. Importantly, the predicted similar structures of other arterivirus members, including equine arteritis virus (EAV), lactate dehydrogenase-elevating virus (LDV), and simian hemorrhagic fever virus (SHFV), also displayed strong IFN induction activities. Together, in this work we identified an innate recognition mechanism by which the PRRSV 3′ UTR pseudoknot region served as PAMPs of arteriviruses and activated innate immune signaling to produce IFNs that inhibit virus replication. All of these results provide novel insights into innate immune recognition during virus infection.

IMPORTANCE PRRS is the most common viral disease in the pork industry. It is caused by PRRSV, a positive single-stranded RNA virus, whose infection often leads to persistent infection. To date, it is not yet clear how PRRSV is recognized by the host and what is the exact mechanism of IFN induction. Here, we investigated the nature of PAMPs on PRRSV and the associated PRRs. We found that the 3′ UTR pseudoknot region of PRRSV, which has been proposed to regulate viral RNA synthesis, could act as PAMPs recognized by RIG-I and TLR3 to induce type I IFN production to suppress PRRSV infection. This report is the first detailed description of pattern recognition for PRRSV, which is important in understanding the antiviral response of arteriviruses, especially PRRSV, and extends our knowledge on virus recognition.

KEYWORDS IFN, PAMPs, PRRSV, PRRs, pseudoknot

Received 28 January 2018 **Accepted** 28 March 2018

Accepted manuscript posted online 4 April 2018

Citation Xie S, Chen X, Qiao S, Li R, Sun Y, Xia S, Wang L-J, Luo X, Deng R, Zhou E-M, Zhang G-P. 2018. Identification of the RNA pseudoknot within the 3′ end of the porcine reproductive and respiratory syndrome virus genome as a pathogen-associated molecular pattern to activate antiviral signaling via RIG-I and Toll-like receptor 3. J Virol 92:e00097-18. https://doi.org/10.1128/JVI.00097-18.

Editor Tom Gallagher, Loyola University Medical Center

Address correspondence to Gai-Ping Zhang, zhanggaiping2003@163.com.

S.X. and X.C. contributed equally to this work.

Virus infections are sensed by host pattern recognition receptors (PRRs) that detect various pathogen-associated molecular patterns (PAMPs) (1, 2). Upon recognition, PRRs activate intracellular signaling pathways that lead to the secretion of interferon (IFN), which induces large amounts of IFN-stimulated genes (ISGs) (3). IFN-α/β are representative cytokines that elicit innate immune responses to establish an antiviral state in infected cells and neighboring noninfected cells and also trigger the adaptive immune response (4–8). Several classes of PRRs have been identified: Toll-like receptors (TLRs), retinoic acid inducible gene I (RIG-I)-like receptors (RLRs), Nod-like receptors (NLRs), and DNA sensors, such as cyclic GMP-AMP synthetase (cGAS), IFN-γ-inducible protein 16 (IFI16), and DEAD box protein 41 (DDX41). Of these PRRs, TLRs and RLRs play a critical role in recognition of RNA virus infection. TLR3, TLR7/8, and TLR9, which localize on the endosomal membrane, recognize double-stranded RNA (dsRNA), single-stranded GU-rich RNA, and DNA with a CpG motif, respectively (4–9). After recognition of viral nucleic acids, TLRs transmit signals to adaptor myeloid differentiation primary response protein 88 (MyD88) or TIR domain-containing adaptor protein inducing IFN-β (TRIF) containing the Toll/interleukin-1 receptor (TIR) domain to activate the transcription factors IFN regulatory factor 3 (IRF3), IRF7, and nuclear factor-κB (NF-κB), which are mainly involved in IFN and proinflammatory gene induction (10). In parallel, the RLRs, which localize in the cytoplasm, are regarded as core sensors in response to RNA virus infection and consist of RIG-I, melanoma differentiation-associated gene 5 (MDA5), and laboratory of genetics and physiology 2 (LGP2) (11). All of the RLR members share a DExD/H-box RNA helicase domain and a C-terminal regulation repressor domain (RD) or C-terminal domain (CTD) (12, 13). In addition, RIG-I and MDA5 harbor two N-terminal caspase recruitment domains (CARDs), which interact with downstream adaptor mitochondrial antiviral signaling protein (MAVS), located in outer mitochondrial membrane (14, 15). This interaction finally activates several transcription factors, IRF3/7 and NF-κB, responsible for IFN and inflammatory gene induction (16). IFN production converges on the induction of ISGs against virus infection, such as IFN-induced protein with tetratricopeptide repeats 1 (IFIT1), dsRNA activated protein kinase R (PKR; also known as eIF2AK2), 2′-5′-oligoadenylate synthetase (OAS), and adenosine deaminase acting on RNA 1 (ADAR1) (17, 18).

As a key PRR, RIG-I was identified as an essential regulator to detect virus-derived RNA during infection with many RNA viruses, such as hepatitis C virus (HCV) and influenza A virus (IAV), whereas MDA5 is crucial for picornavirus sensing (11, 15, 19–27). However, some viruses, such as dengue virus (DV; positive single-stranded RNA [ssRNA]), West Nile virus (WNV; positive-sense ssRNA), measles virus (MeV; negative-sense ssRNA), and reovirus (dsRNA) were reported to be sensed by both RIG-I and MDA5 (19, 28–31). This non-self-recognition largely depends on the features of foreign nucleic acids, such as nucleic acid sequences and RNA secondary structures (32). It is now well established that RIG-I detects ssRNA bearing a hairpin structure with a natural 5′-triphosphate (5′-ppp), such as the panhandle structure of IAV, as major signatures (15, 33), since most host cytosolic RNAs are modified by cleavage or capping (34–37). However, base-paired 5′pp-RNAs can also serve as RIG-I agonists (38). Overall, more detailed studies are urgently needed to classify the exact mechanism of different PAMPs during viral infection (39).

Porcine reproductive and respiratory syndrome virus (PRRSV), an enveloped single-stranded positive-sense RNA virus, belongs to the *Arteriviridae* family, order *Nidovirales*. PRRSV contains two genotypes, type 1 (European type) and type 2 (North American type) (40). The PRRSV genome is approximately 15.4 kb and encodes at least 10 open reading frames (ORFs) that containing two polyprotein precursors (pp1a and pp1ab) and 8 structural proteins (glycoprotein 2a [GP2a], GP2b, GP3, GP4, GP5a, GP5, the matrix protein M, and the nucleocapsid [N] protein) (41, 42). pp1a and pp1ab can be cleaved into at least 16 nonstructural proteins (nsps), including nsp1α, nsp1β, nsp2 to -6, nsp2TF, nsp2N, nsp7α, nsp7β, and nsp8 to -12. PRRSV mainly targets primary porcine alveolar macrophages (PAMs) during acute infection *in vivo*. Numerous studies have reported that PRRSV does not induce a strong IFN response (43, 44). However, PRRSV

is sensitive to IFNs, which is demonstrated *in vitro* and *in vivo* (45, 46). Notably, it has been reported that PRRSV induces IFN-β mRNA expression in both PAMs and monocyte-derived dendritic cells (MDDCs) *in vitro* (47, 48). Moreover, IFN induction activities differ among PRRSV isolates (44). Therefore, it is essential to assess the innate immune response against PRRSV infection in detail, especially type I IFN response. In addition, further studies are necessary to clarify how PRRSV is recognized by porcine immune cells and the underlying sensing mechanism of type I IFN induction. The exact nature of PAMPs on PRRSV and the host-associated PRRs have not been described yet. Here, we investigated IFN and ISG production as well as the PRRs related to PRRSV infection. We found that PRRSV mainly induced type I, but not type III, IFNs in PAMs, and RIG-I and TLR3 were essential for PRRSV recognition and IFN induction. Interestingly, we found that the pseudoknot of the PRRSV 3′ untranslated region (UTR), which functions in RNA synthesis and virus replication, served as a PAMP and directly bound to RIG-I to stimulate IFN induction. To gain further insights into the contributions of the 3′ UTR pseudoknot, we disrupted the pseudoknot interaction between the two terminal stem-loop structures by introducing nucleotide mutation without affecting the predicted structure of the individual hairpins. We found that the pseudoknot variants exhibited much weaker IFN response. Furthermore, the 3′ UTR pseudoknot RNA transcripts of PRRSV suppressed PRRSV replication in PAMs. More importantly, the predicted similar structures of equine arteritis virus (EAV), lactate dehydrogenase-elevating virus (LDV), and simian hemorrhagic fever virus (SHFV) exhibited similar effects. Collectively, our data are the first to describe the innate recognition mechanism during capped virus PRRSV infection by which the pseudoknot structure in the 3′ UTR functions as a PAMP, chiefly interacting with host sensor RIG-I and TLR3 to activate the antiviral immune response.

RESULTS

PRRSV induces an antiviral response in PAMs. To fully understand the innate immune response during PRRSV infection, we primarily assessed the ability of PRRSV to induce IFN types I (IFN-α and IFN-β), II (IFN-γ), and III (IFN-λ1) in CRL2843-CD163 and PAMs with different strains of PRRSV, using quantitative reverse transcription-PCR (qRT-PCR) and luciferase reporter assay. Our results showed that PRRSV significantly increased IFN-β mRNA production in porcine macrophage cell line CRL2843-CD163 upon HN07-1 and BJ-4 infection. Furthermore, IFN-β induction was dose dependent, as represented by BJ-4 infection (Fig. 1A and B). Dose-dependent IFN-β increase in CRL2843-CD163 cells was also confirmed by Dual-Luciferase assay (Fig. 1C). Consistent with these results, IFN-β and IFN-α levels were upregulated after BJ-4 infection and peaked at 12 h postinfection (hpi) (192-fold and 17.1-fold, respectively) in PAMs. Similar kinetic trends were observed with highly pathogenic PRRSV (HP-PRRSV) strain HN07-1 (Fig. 1D). However, IFN-β and IFN-α induction by HN07-1 peaked at 24 (191-fold) and 48 (5.34-fold) hpi, respectively, indicative of a later and lower effect than that of BJ-4 (Fig. 1D). A slight increase of IFN-γ and IFN-λ1 was not observed until 6 hpi or 12 hpi with BJ-4 and HN07-1. These results indicated a difference in IFN induction between HP-PRRSV HN07-1 and PRRSV strain BJ-4 (Fig. 1D). Meanwhile, we also evaluated the induction of PKR, OAS, ISG56, and MX1 by PRRSV. All of them were upregulated after PRRSV infection and peaked at 24 hpi (Fig. 1E). In addition, the induction of type I IFN mRNA was probably replication dependent, because UV-inactivated and heat-inactivated BJ-4 failed to induce IFN-β, IFN-α, MX1, and ISG56 mRNA expression, unlike live BJ-4 (Fig. 1F). PRRSV RNA was quantified in live and inactivated PRRSV-inoculated cells and culture supernatants by qRT-PCR. PRRSV RNA was detected at 6 hpi and continued to increase rapidly at 12 hpi before decreasing at 24 hpi in BJ-4-infected cells, while it had a sustained increase in supernatant after BJ-4 infection. In contrast, PRRSV RNA was hardly observed in cells and supernatant upon UV- or heat-activated BJ-4 treatment (Fig. 1F). These data confirmed efficient live PRRSV replication in PAMs and successful inactivation of PRRSV via UV or heat inactivation. Our result indicated the significant induction of IFN and ISGs after infection with PRRSV in PAMs. Moreover,

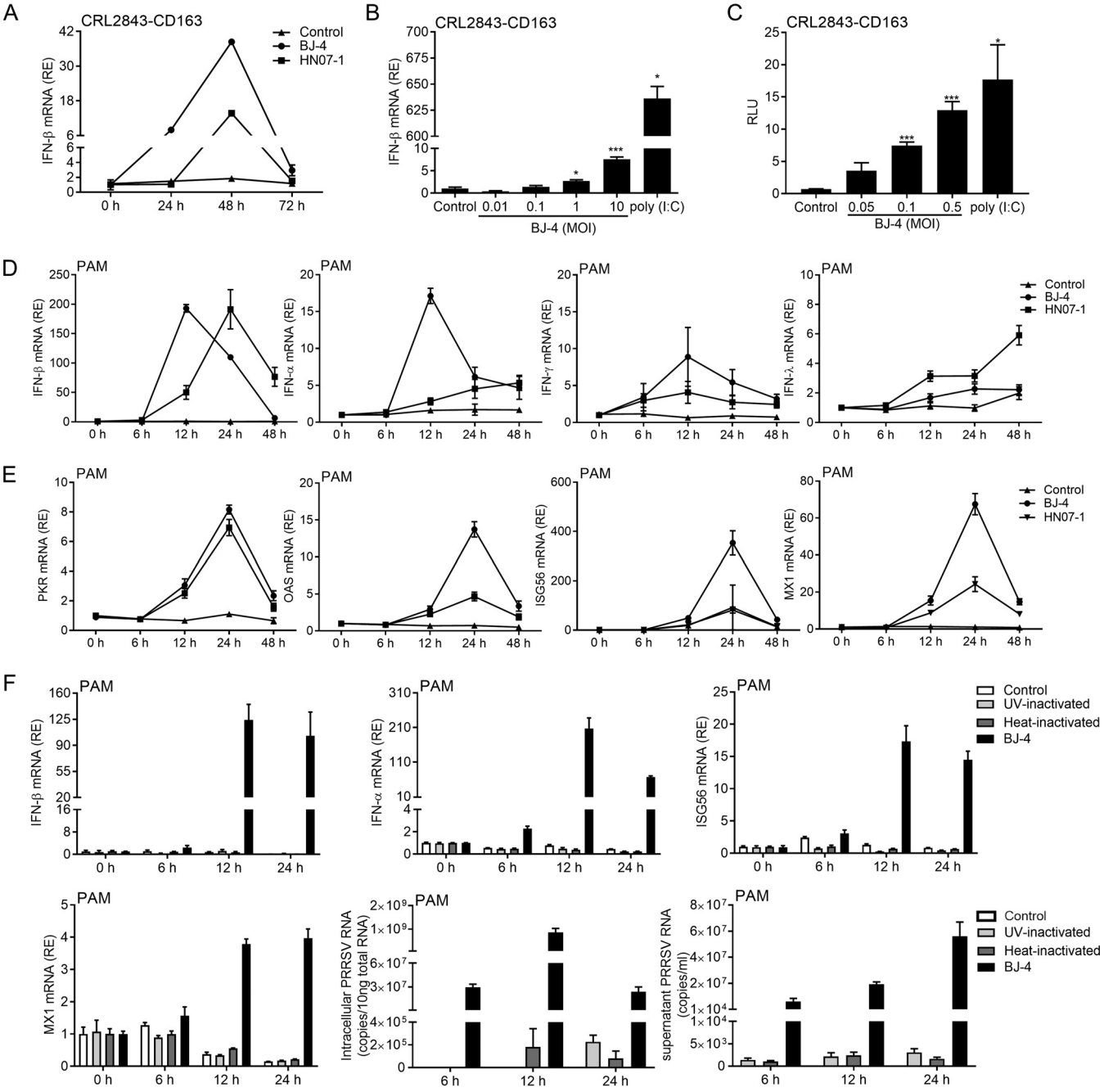

FIG 1 IFN induction in CRL2843-CD163 and PAMs in response to PRRSV infection. (A) CRL2843-CD163 cells were either mock infected (control) or infected with PRRSV BJ-4 or HN07-1 (MOI of 1.0). At 24, 48, and 72 hpi, the IFN-β mRNA levels in the cells were determined by qRT-PCR. (B) CRL2843-CD163 cells were either mock infected (control) or infected with the PRRSV BJ-4 at MOIs of 0.01, 0.1, 1.0, and 10. At 24 hpi, the IFN-β mRNA levels in the cells were determined by qRT-PCR. Transfection of 1 μg poly(I·C) was used as a positive control. (C) CRL2843-CD163 cells were transfected with 1 μg IFN-β-Luc and 100 ng pRL-TK renilla luciferase reporter plasmid, followed by infection with the PRRSV BJ-4 at an MOI of 0.05, 0.1, and 0.5, respectively, or transfection of 1 μg poly(I·C). At 24 hpi, the IFN-β reporter levels in the cells were determined by luciferase activity. (D and E) PAMs were mock infected (control) or infected with the PRRSV BJ-4 or HN07-1 (MOI of 1). Total RNA was extracted from cell lysates. IFN-β, IFN-α, IFN-γ, IFN-λ1, PKR, OAS, ISG56, and MX1 were quantified by qRT-PCR at the indicated times. (F) PAMs were mock infected (control) or infected with PRRSV strain BJ-4 (MOI of 1), UV-inactivated, heat-inactivated BJ-4 in PAMs. IFN-β, IFN-α, ISG56, and MX1 were quantified by qRT-PCR at the indicated times. Viral copy numbers were performed by analysis of ORF7 RNA levels. RE, relative expression. RLU, relative luciferase units. Data are expressed as means ± SEM from three independent experiments. *P* values were calculated using Student's *t* test. *, $P < 0.05$; **, $P < 0.01$; ***, $P < 0.001$.

some genes induced by HN07-1 exhibited a delayed and lower response compared with that of the BJ-4 strain.

RIG-I, MDA5, and TLR3 are involved in PRRSV-induced IFN-β induction. We next examined which PRR signaling pathways were answerable for the PRRSV-induced IFN

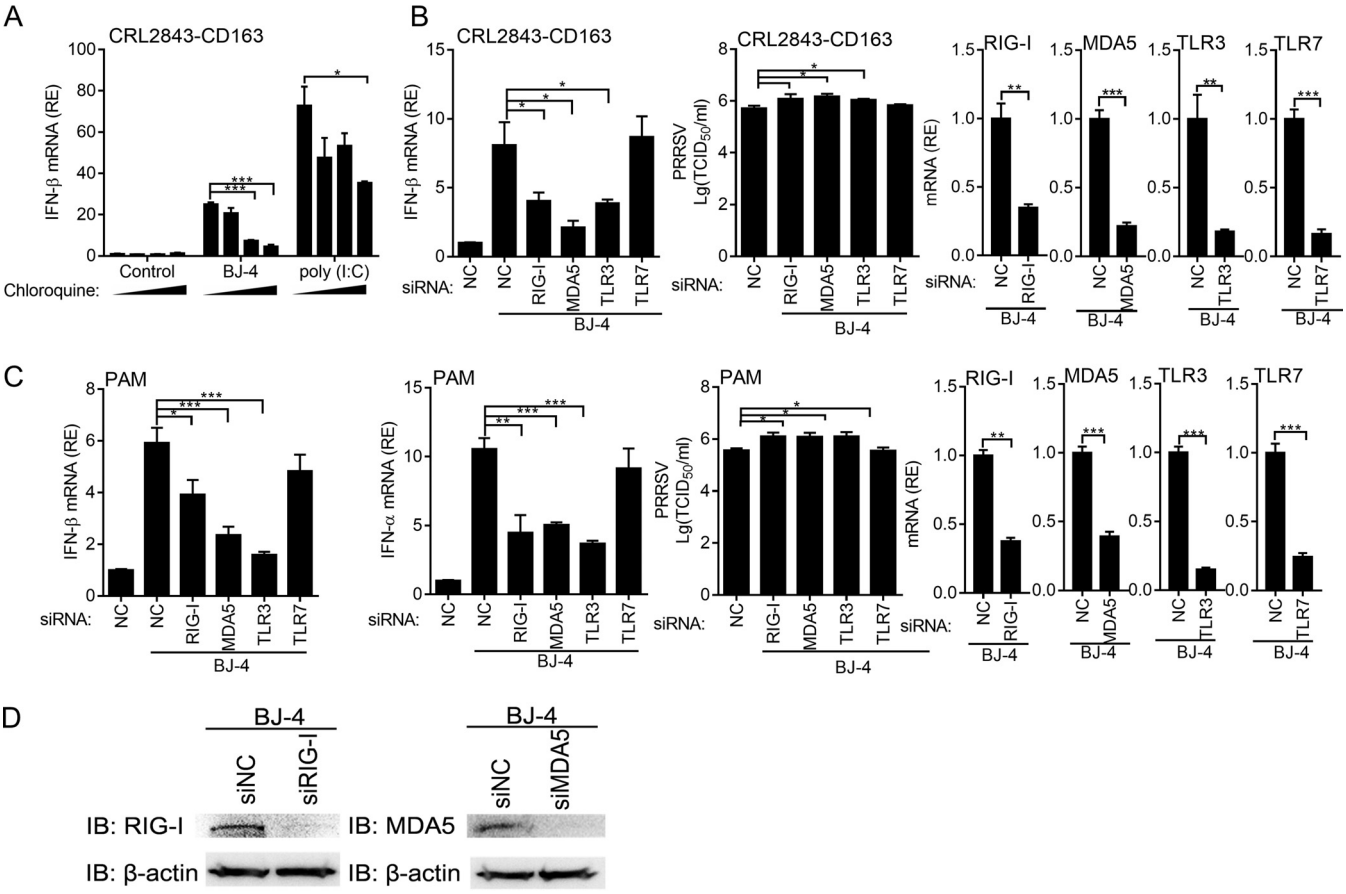

FIG 2 IFN induction by PRRSV is dependent on RIG-I, MDA5, and TLR3. (A) CRL2843-CD163 cells were pretreated with 0 μM, 20 μM, 40 μM, or 80 μM chloroquine for 1 h, followed by infection with PRRSV BJ-4 (MOI of 1) after 24 h or transfection with 1 μg poly(I·C) for 24 h in the presence of inhibitor. IFN-β mRNA production was determined by qRT-PCR. (B) CRL2843-CD163 cells were treated with control siRNA (NC) or the indicated siRNAs against RIG-I, MDA5, TLR3, and TLR7 and then infected with PRRSV BJ-4 (MOI of 1). At 36 hpi, total RNAs were subjected to qRT-PCR analysis for IFN-β mRNA, and the supernatants were collected for $TCID_{50}$ determination. Knockdown efficiency was analyzed by qRT-PCR. (C and D) PAMs were treated with control siRNA (NC) or the indicated siRNAs and then infected with PRRSV BJ-4 (MOI of 0.5). (C) At 12 hpi, total RNAs were subjected to qRT-PCR analysis for IFN-β, and IFN-α mRNA and the supernatants were collected for $TCID_{50}$ determination. Knockdown efficiency was analyzed by qRT-PCR (C) and Western blotting (D). RE, relative expression; IB, immunoblot. Data are expressed as means $\pm$ SEM from three independent experiments. *P* values were calculated using Student's *t* test. *, $P < 0.05$; **, $P < 0.01$; ***, $P < 0.001$.

response. Since PRRSV is a single-stranded, positive-sense RNA virus (49), we evaluated the contribution of previously reported cytosolic RNA sensors RIG-I and MDA5 and endosomal RNA sensors TLR3 and TLR7. We first analyzed the involvement of endosomal PRRs in PRRSV-induced IFN-β production by using chloroquine, an endosomal acidification inhibitor, which could inhibit TLR enzymatic activity (50). As shown in Fig. 2A, chloroquine pretreatment showed a dose-dependent inhibitory effect on PRRSV-induced IFN-β response, the same as that induced by poly(I·C), which depended on TLR3 in macrophages (51). Thus, endosomal TLR3/7 were relevant to PRRSV-induced IFN-β production (Fig. 2A). We next used short interfering RNA (siRNA) to specifically knock down endogenous expression of TLR3/7 as well as the cytosolic RNA sensors RIG-I and MDA5. The effects of these gene knockdowns on IFN-β induction were evaluated. As shown in Fig. 2B, decreased expression of RIG-I, MDA5, and TLR3, but not TLR7, significantly dampened IFN-β expression in CRL2843-CD163. Moreover, PRRSV titers in the supernatant were assessed by 50% tissue culture infectious dose ($TCID_{50}$) assay. Decreased expression of RIG-I, MDA5, and TLR3, but not TLR7, significantly increased the viral yields at least 2.18-fold compared to that of control CRL2843-CD163 cells. Interference effects of siRNA were assessed by qRT-PCR to analyze RNA levels of targeted proteins (Fig. 2B). We then performed the same experiments with PAMs. Similar results were observed for siRNA against RIG-I, MDA5, and TLR3, which markedly

reduced IFN-β and IFN-α expression (Fig. 2C). PRRSV titers in the supernatant were also assessed by $TCID_{50}$ assay. Decreased expression of RIG-I, MDA5, and TLR3, but not TLR7, significantly increased the viral yields at least 3.8-fold compared to that of the control. Interference effects of siRNA were assessed by qRT-PCR and immunoblotting to analyze RNA and protein level of targeted proteins (Fig. 2C and D). Note that TLR3 and TLR7 protein levels were unable to be detected due to a lack of relevant porcine antibodies. Taken together, these results suggest that IFN induction by PRRSV is dependent on cytosolic sensors RIG-I, MDA5, and endosomal TLR3.

The 3′ UTR pseudoknot region of PRRSV genome RNA is a key element for IFN induction. RNA with complicated secondary structures, such as the panhandle structure of IAV, is very effective for PAMP recognition and innate immune activation (33). Because the 5′ UTR and 3′ UTR of the PRRSV genome are highly structured and the subgenomic mRNAs of arteriviruses possess nested 3′ cotermini, we hypothesized that they played a vital role in PRRSV recognition. We then utilized an *in vitro* transcription system to generate the entire 5′ UTR and 3′ UTR of PRRSV and characterized their immunoreactivities by transfection into PAMs (52, 53). As expected, transfection of 5′ UTR and 3′ UTR induced IFN-β and IFN-α with a dose-dependent increase (Fig. 3A and B). In order to further investigate the specific region of 5′ UTR and 3′ UTR that is responsible for IFN induction, we predicted the secondary structures of the 5′ UTR and 3′ UTR and searched for possible structural elements residing in PRRSV 5′ UTR and 3′ UTR RNA by *in silico* analysis using Mfold software (54, 55). As shown in Fig. 3C and D, the predicted schematic representation of the 5′ UTR and 3′ UTR of BJ-4 suggested that the BJ-4 5′ UTR possessed 5 stem-loop structures, and the 3′ UTR possessed 2 bulged stem-loop structures. Based on this prediction, we synthesized five truncated mutants (1-47, 46-79, 71-108, 107-158, and 155-190) of the 5′ UTR and three truncated mutants of the 3′ UTR (1-16&131-151, 15-84, and 79-131) to test their immune-stimulatory abilities in PAMs and CRL2843-CD163. The results showed that none of these eight fragments showed IFN-β increase in CRL2843-CD163 or PAMs (Fig. 3E and F).

RNA secondary prediction by the program Mfold is mainly based on the principle of energy minimization (56, 57), and the method was widely used to predict the RNA secondary structures. Therefore, we gave priority to the predicted structure of PRRSV 5′ UTR and 3′ UTR RNA. Due to the inability of inducing IFN response by these truncated fragments, shown with IFN-β (Fig. 3E and F), we then analyzed whether other structures could act as PAMPs responsible for PRRSV recognition. An alternative structure is demonstrated to be formed during the course of viral replication (58–62). This alternative structure of the PRRSV 3′ UTR containing an RNA pseudoknot interaction between the two terminal stem-loop structures was characterized as a molecular switch in viral RNA synthesis (58). Moreover, IFN induction by PRRSV correlated with virus replication (Fig. 1F). Thus, we suspect that the pseudoknot would act as a PAMP responsible for PRRSV recognition (Fig. 4A). The truncated fragments of this 3′ UTR structure containing the pseudoknot (1-49, 50-88, 89-151, 1-88, and 50-151) were synthesized by *in vitro* transcription. Their immunoactivities then were detected by transfection into PAMs. The results indicated that those truncated fragments and the entire 3′ UTR could induce IFN-β and IFN-α mRNA expression to different degrees in PAMs after transfection at 6 h and 12 h (Fig. 4B and C). The 50-151 fragment, also designated the pseudoknot structure, induced the most IFN-β. The data from luciferase reporter assay in Marc-145 cells also confirmed this conclusion that the pseudoknot fragment of PRRSV BJ-4 3′ UTR induced significantly higher luciferase activity than the control (Fig. 4D). Subsequently, PAMs were transfected with the 3′ UTR 1-151 or the pseudoknot fragment of BJ-4 for 0, 6, 12, and 24 h. The results indicated that the pseudoknot fragment of BJ-4 significantly increased IFN-β, IFN-α, and ISG56 mRNA production (Fig. 4E). To gain further insight into whether the IFN stimulatory activities was dependent on virus strain, we compared the IFN stimulatory activities of the pseudoknot fragment of HP-PRRSV strain HN07-1 and low-pathogenicity PRRSV strain BJ-4 using different doses (0.125, 0.25, 0.5, or 1 μg). The pseudoknot fragments of BJ-4 and HN07-1 largely increased IFN-β, IFN-α, and ISG56 mRNA expression at 6 h and 12

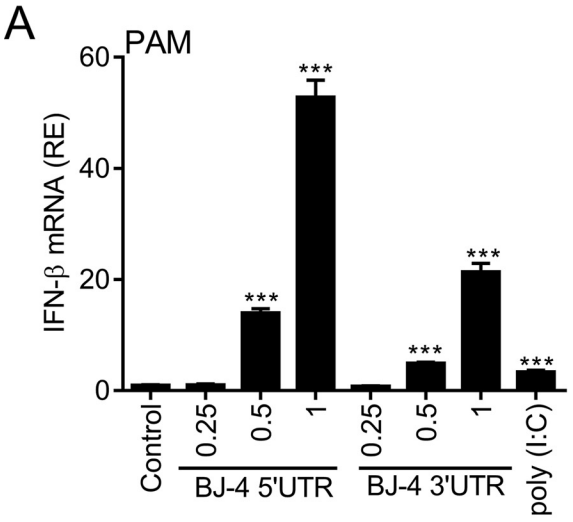
A
PAM
IFN-β mRNA (RE)
60
40
20
0
***
Control
0.25
0.5
1
BJ-4 5'UTR
BJ-4 3'UTR
poly (I:C)

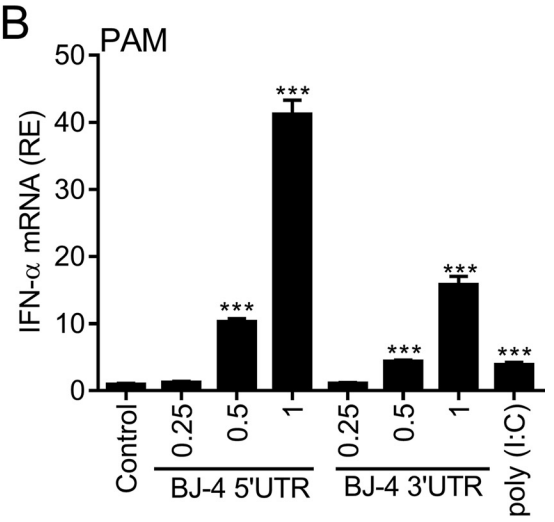
B
PAM
IFN-α mRNA (RE)
50
40
30
20
10
0
***
Control
0.25
0.5
1
BJ-4 5'UTR
BJ-4 3'UTR
poly (I:C)

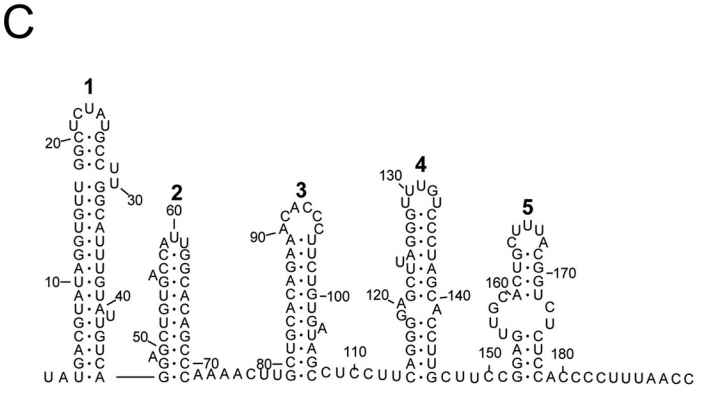
C
1
2
3
4
5

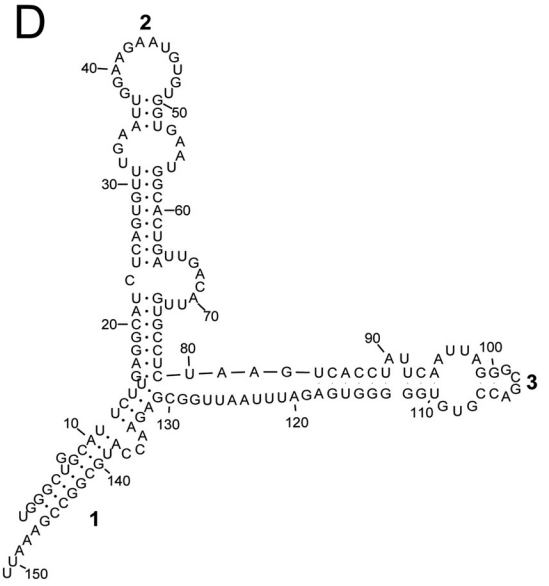
D
1
2
3

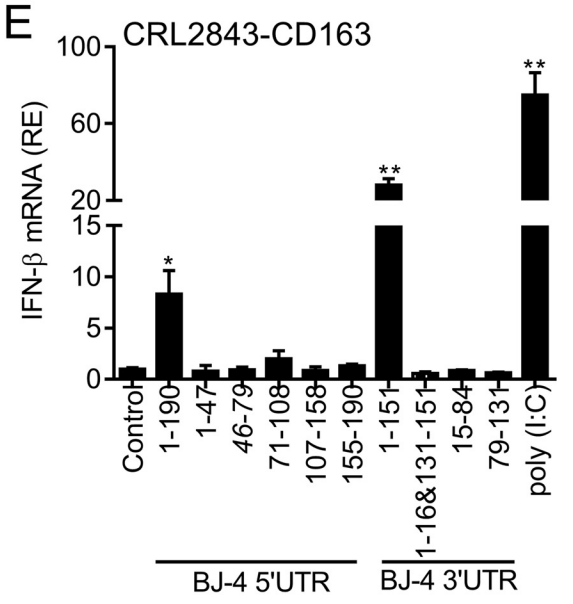
E
CRL2843-CD163
IFN-β mRNA (RE)
100
60
20
15
10
5
0
*
**
**
Control
1-190
1-47
46-79
71-108
107-158
155-190
1-151
1-16&131-151
15-84
79-131
poly (I:C)
BJ-4 5'UTR
BJ-4 3'UTR

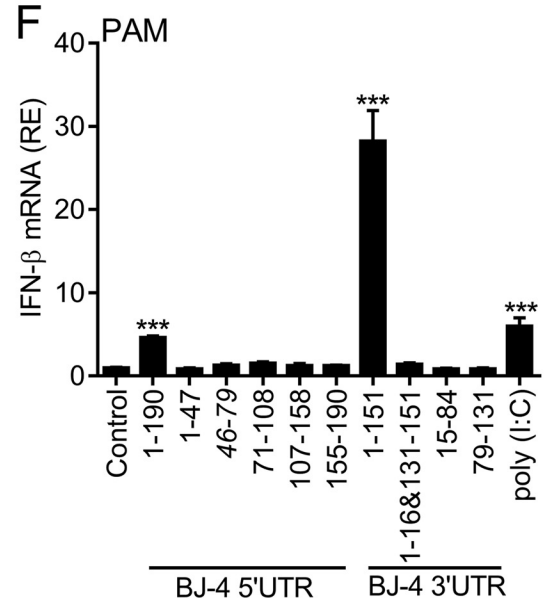
F
PAM
IFN-β mRNA (RE)
40
30
20
10
0
***
***
***
Control
1-190
1-47
46-79
71-108
107-158
155-190
1-151
1-16&131-151
15-84
79-131
poly (I:C)
BJ-4 5'UTR
BJ-4 3'UTR

h (Fig. 4F and G). IFN-β, IFN-α, and ISG56 mRNA induction in PAMs by the pseudoknot fragments was in a dose-dependent but PRRSV strain-independent manner.

The pseudoknot interaction is critical for strong IFN induction. To investigate whether the formation of pseudoknot interaction was crucial for IFN induction, several mutants of pseudoknot residing in the BJ-4 3′ UTR, disrupting the interactions without affecting the structure of the unique hairpins, were generated as previously described on EAV (58). In the mutants SW1 and SW2, we switched the seven nucleotides in the core of SL1 and SL2, respectively. The base pairing was restored in double mutant SW12 by exchanging the seven nucleotides in the core of SL1 and SL2 simultaneously. In the other set, the orientation of central seven nucleotides in SL1 and SL2 was changed in mutants OR1 and OR2, respectively, or both changed in mutant OR12, which restored the base-pairing possibilities (Fig. 5A). These mutants and the original pseudoknot were transfected in PAMs for 6 h or 12 h, and their effects on IFN induction were determined. As shown in Fig. 5B and C, the variants (SW1, SW2, OR1, and OR2) carrying mutations of disruption of pseudoknot interaction dramatically dampened IFN induction both at 6 h and 12 h. The mutants OR12 and SW12 showed the most robust IFN-β and IFN-α mRNA response, similar to that of the original pseudoknot structure, which indicated that it was important for the induction by the original pseudoknot structure (Fig. 5B and C). Taken together, these results demonstrated that the pseudoknot interactions between terminal loop regions and the upstream hairpin contributed efficiently to IFN induction.

Both RIG-I and TLR3 are required for the pseudoknot to induce IFN response. To delineate which PRRs are dominant in pseudoknot sensing to relay the signal for antiviral response, we used siRNA to silence the endogenous expression of each receptor. We found that siRNA targeting RIG-I and TLR3 markedly reduced IFN-β, IFN-α, ISG56, and MX1 expression in PAMs transfected with pseudoknot of BJ-4, whereas siRNA targeting MDA5 and TLR7 did not (Fig. 6A to D). Knockdown efficiency of siRNA examined by qRT-PCR was around 60% (Fig. 6E). The protein levels of RIG-I and MDA5 were also detected (Fig. 6F). Overall, these data suggested that the signaling cascades leading to IFN-β, IFN-α, ISG56, and MX1 mRNA induction by the pseudoknot of the BJ-4 3′ UTR are initiated by RIG-I and TLR3.

RIG-I and TLR3 interact with the pseudoknot of PRRSV 3′ UTR. We next investigated whether RIG-I and TLR3 interacted with the pseudoknot regions of the PRRSV 3′ UTR. The HEK293T cells were transfected with the plasmid encoding Flag-pRIG-I. After being lysed, cells were incubated with biotinylated RNA as indicated and subjected to pulldown. Previous studies have demonstrated that the 5′-triphosphate end of RNA generated by viral polymerases is responsible for RIG-I recognition, and the 5′ terminal modification of the RNA is very important for RIG-I recognition (34, 63). 5′-Triphosphate-terminated 3pRNA as a RIG-I ligand was used as a positive control (34), and the capped ContRNA was used as a negative control (54). As shown in Fig. 7A, the Flag-pRIG-I in HEK293T cells was coprecipitated with the pseudoknot of BJ-4 3′ UTR labeled with biotinylated nucleotide as well as 3pRNA but not with the labeled ContRNA, indicating that Flag-pRIG-I specifically interacted with the pseudoknot of the BJ-4 3′ UTR. RIG-I is composed of three main structural domains: two CARD domains at the N terminus for signal transduction, the central DExD/H box RNA helicase domain and C-terminal domain (RD) for RNA binding (12, 15). To further define the specific domains of RIG-I associated with the pseudoknot, RNA pulldown assay with several deletion mutants of pRIG-I was performed. The results strongly suggested that the C-terminal portion of RIG-I (pRIG-I-RD) and not the CARDs bound to the pseudoknot

FIG 3 Full-length 5′ and 3′ UTR of PRRSV induce an IFN response. (A and B) PAMs were transfected with the entire 5′ UTR or 3′ UTR transcripts of PRRSV BJ-4 at different doses (0.25, 0.5, or 1 μg), poly(I·C) (1 μg), or the no-RNA control. At 6 h posttransfection, RNA was isolated to determine IFN-β and IFN-α mRNA levels by qRT-PCR. (C and D) A schematic representation of 5′ UTR and 3′ UTR of BJ-4 was shown. (E and F) CRL2843-CD163 or PAMs were transfected with 1 μg of 5′ UTR or 3′ UTR truncated transcripts of PRRSV BJ-4 genome, poly(I·C), or the no-RNA control for 6 h. The IFN-β mRNA levels in the cells then were analyzed by qRT-PCR. RE, relative expression. Data were expressed as means ± SEM from three independent experiments. *P* values were calculated using Student's *t* test. *, $P < 0.05$; **, $P < 0.01$; ***, $P < 0.001$.

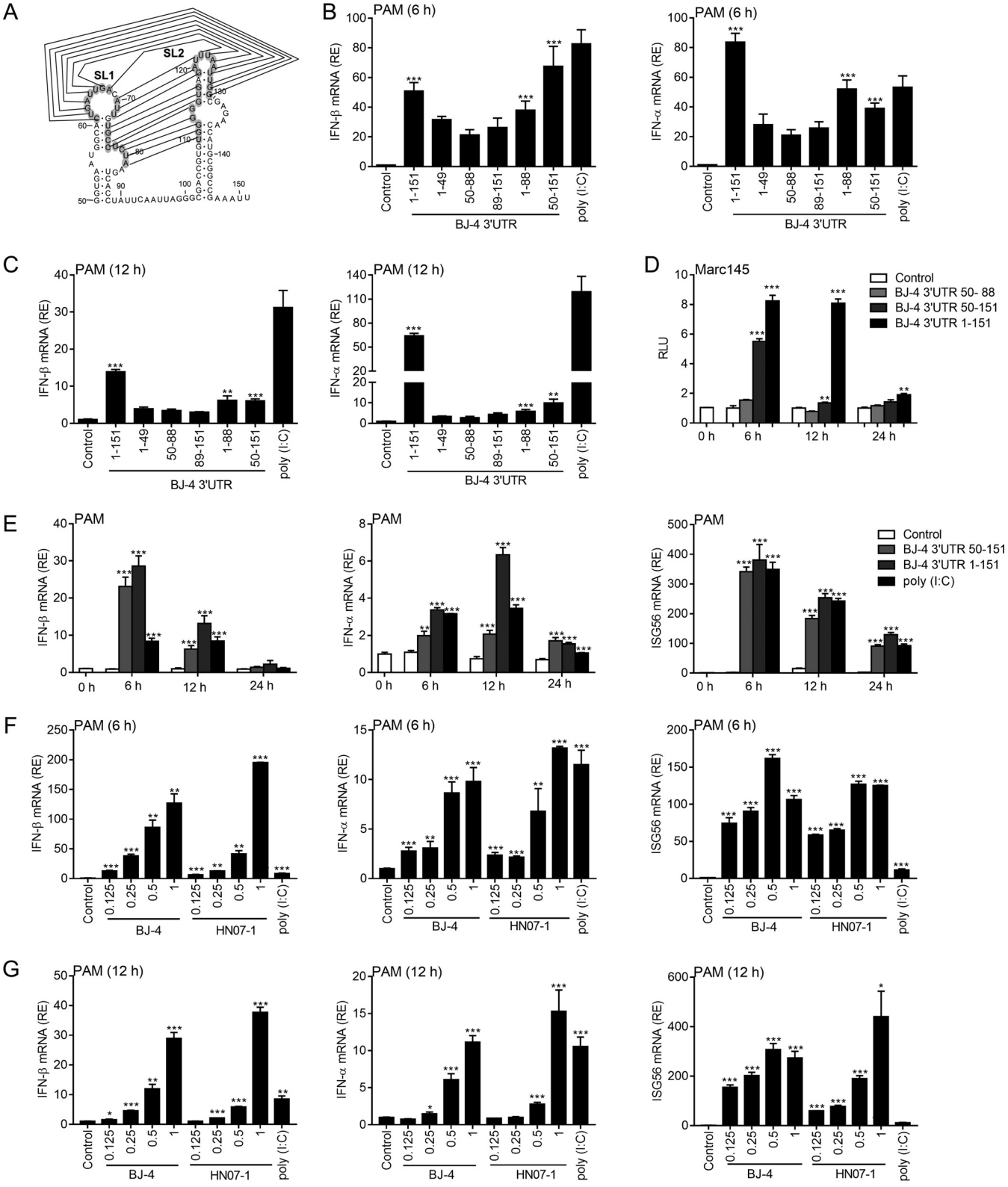

FIG 4 3′ UTR pseudoknot transcripts of PRRSV BJ-4 induce an antiviral response. (A) A schematic representation of 3′ UTR pseudoknot of PRRSV BJ-4. The nucleotides involved in the pseudoknot interaction are marked in gray, and the base-pairing interaction is depicted by lines. (B and C) PAMs were transfected with 1 μg of 3′ UTR-truncated transcripts of the PRRSV BJ-4 genome (1-151, 1-49, 50-88, 89-151, 1-88, and 50-151 [pseudoknot]) for 6 h or 12 h, and the IFN-β and IFN-α mRNA levels in the cells were analyzed by qRT-PCR. (D) Marc145 cells were cotransfected with plasmids encoding constitutive renilla luciferase and IFN-β promoter firefly luciferase construct. After 24 h, the cells were transfected with 1 μg of the indicated RNA (BJ-4 3′ UTR 1-151, BJ-4 3′ UTR pseudoknot, and BJ-4 3′ UTR 50-88) constructs or control. Cells were harvested 0, 6, 12, or 24 h later for dual-luciferase assay. (E) PAMs were transfected with 1 μg of 3′ UTR 1-151 or 3′ UTR pseudoknot transcripts of PRRSV BJ-4 genome for 6 h, 12 h, or 24 h, and the IFN-β, IFN-α and ISG56 mRNA levels in the cells were analyzed

(Continued on next page)

labeled by biotinylated nucleotide (Fig. 7B). We also probed which region of pTLR3 bound to the pseudoknot of the BJ-4 3′ UTR. The results indicated that the ectodomain of pTLR3 (pTLR3-ECD) interacted with the pseudoknot labeled by biotinylated nucleotide but not the cytoplasm of pTLR3 (pTLR3-TIR). Taken together, these data demonstrated a strong and specific interaction between the pseudoknot region of the BJ-4 3′ UTR and RIG-I and TLR3, which may trigger downstream signaling to induce IFN response.

In order to further understand the interaction of pRIG-I-RD and BJ-4 3′ UTR pseudoknot RNA transcripts, we performed an RNA binding assay on pRIG-I-RD by gel filtration chromatography. The BJ-4 3′ UTR pseudoknot RNA transcripts were synthesized by *in vitro* transcription as mentioned above. The pRIG-I-RD protein was expressed in *Escherichia coli* Transetta and purified. The chromatography assay indicated that the BJ-4 3′ UTR pseudoknot RNA transcripts bound to pRIG-I-RD and formed stable complexes (Fig. 7C).

The PRRSV 3′ UTR pseudoknot RNA transcripts restrict PRRSV replication in PAMs. Based on the IFN stimulatory activities, we speculated that the pseudoknot of the PRRSV 3′ UTR had an anti-PRRSV effect. Thus, following transfection with the pseudoknot or the mutant SW1 transcripts for 24 h, PAMs were inoculated with BJ-4 (MOI of 1) for 12 h or 18 h. In the supernatant, PRRSV titer and RNA copies were assessed by $TCID_{50}$ and absolute qRT-PCR, respectively. Meanwhile, RNA copies in cells were also quantified. As shown in Fig. 8A to C, transfection with pseudoknot segments significantly suppressed PRRSV replication in PAMs. The pseudoknot segments reduced the viral yields at least 2-fold compared to those of control cells at 12 hpi or 18 hpi in supernatant. In contrast, the pseudoknot mutant SW1 showed no inhibiting effects on PRRSV titer at 12 hpi and weakly inhibiting effect at 18 hpi (Fig. 8A). The PRRSV copies in the supernatants after transfection with the pseudoknot segments were also suppressed at least 1.4-fold at 12 hpi and 4.9-fold at 18 hpi compared to that of control cells. In contrast, the PRRSV RNA copies in the supernatants after transfection with the SW1 pseudoknot mutants showed no obvious changes compared to that of the control but showed significant difference compared to that of the BJ-4 3′ UTR pseudoknot (Fig. 8B). Transfection with the pseudoknot segment, but not the mutant SW1, significantly downregulated the PRRSV copies in PAMs at 12 hpi and 18 hpi compared to that in control cells (Fig. 8C). Therefore, the pseudoknot exhibited a stronger anti-PRRSV effect in PAMs than the mutant SW1.

Simultaneously, the mRNA expression of IFN-β, IFN-α, and ISG56 was detected. Our results showed that transfection with the pseudoknot segment increased IFN-β, IFN-α, and ISG56 production compared to that of the control at 12 hpi and 18 hpi. However, the pseudoknot mutant SW1-induced IFN-β, IFN-α and ISG56 mRNA expression levels were significantly reduced compared with those of the pseudoknot (Fig. 8D to F). Taken together, the results suggested that PRRSV 3′ UTR pseudoknot segments could induce significant IFN-α, IFN-β, and ISG56 expression and have an anti-PRRSV effect.

The IFN stimulatory activity of the PRRSV 3′ UTR pseudoknot is conserved among all known arteriviruses. The pseudoknot interaction is conserved among members of arteriviruses, including EAV, LDV, SHFV, and PRRSV (58). In order to identify the sequence conservation of the proposed pseudoknot interaction, alignment of the 3′ end of different arteriviruses was performed (Fig. 9A). The pseudoknot interaction regions of PRRSV strains BJ-4 and A2MC2 were identical to that of the standard isolate VR-2332. For HN07-1, 15GD1, Ingelvac, HB-1, and HB-2 strains we observed a U-C mutation in SL1 and an A-G mutation in SL2, which might confer a new G-C base pairing (bases marked with gray lines). The C-U mutation in SL1 and G-A mutation in

FIG 4 Legend (Continued)

by qRT-PCR. (F and G) PAMs were transfected with 0.125, 0.25, 0.5, and 1 μg of the 3′ UTR pseudoknot transcripts of PRRSV BJ-4 or HN07-1 genome for 6 h (F) or 12 h (G), and the IFN-β, IFN-α, and ISG56 mRNA levels were analyzed by qRT-PCR. Transfection of 1 μg poly(I·C) was used for a positive control. Control stands for the no-RNA treatment. RE, relative expression. Data are expressed as means ± SEM from three independent experiments. *P* values were calculated using Student's *t* test. *, $P < 0.05$; **, $P < 0.01$; ***, $P < 0.001$.

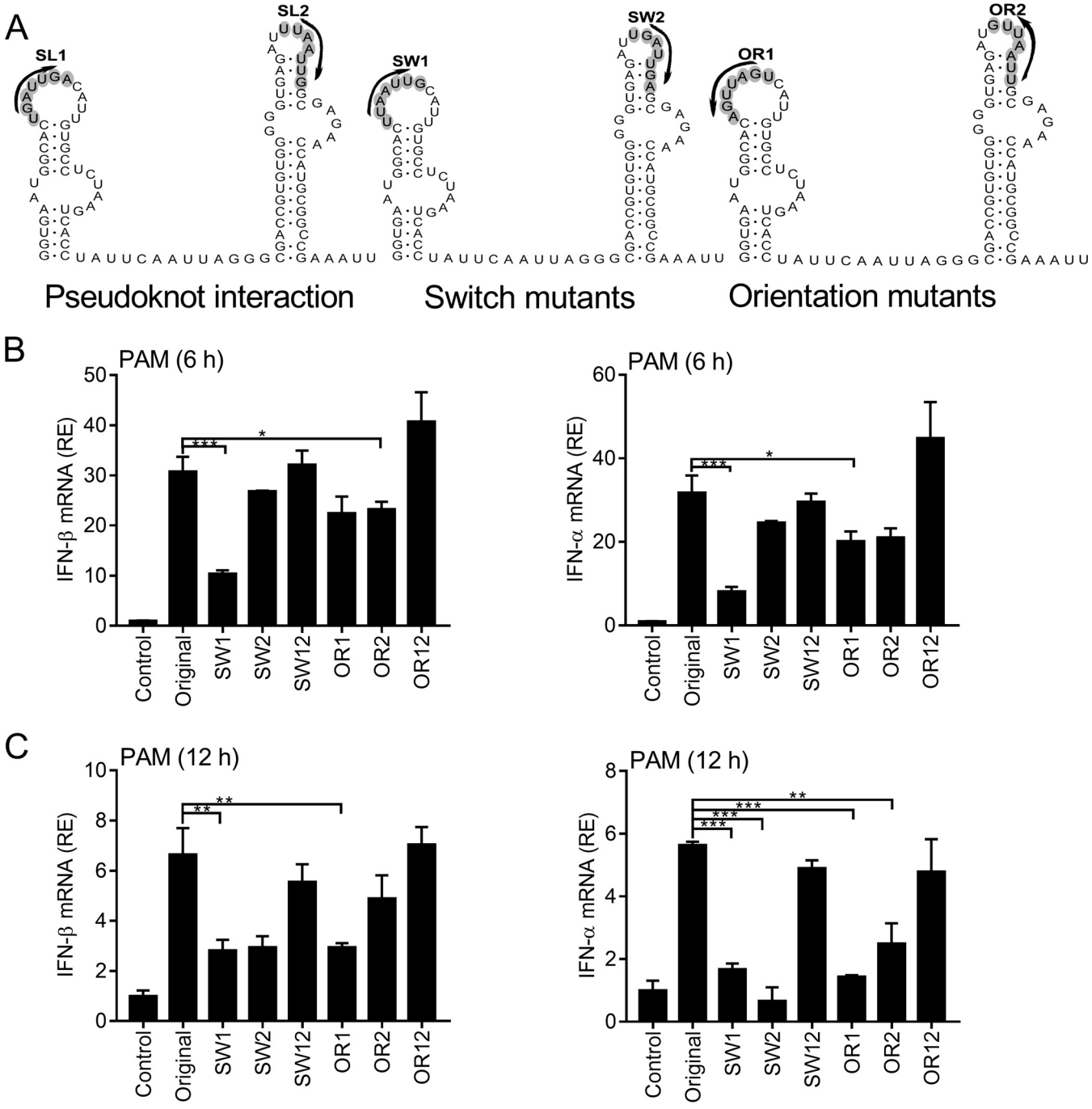

FIG 5 Pseudoknot mutations significantly weaken IFN stimulatory activity. (A) A schematic representation of BJ-4 3′ UTR pseudoknot mutant transcripts. The seven nucleotides of SL1 were switched with those of SL2 in mutant SW1 and vice versa in mutant SW2. The base-pairing possibilities were restored in mutant SW12 by switching the seven nucleotides. The mutants OR1 and OR2 were generated by changing the orientation of the central seven nucleotides in the loop of SL1 or SL2. The orientation of the central seven nucleotides was changed in mutant OR12, which restored the base-pairing possibilities. (B and C) PAMs were transfected with 3′ UTR pseudoknot wild-type or mutant transcripts of PRRSV BJ-4 genome constructs or the no-RNA control for 6 h (B) or 12 h (C), and the IFN-β and IFN-α mRNA levels were analyzed by qRT-PCR. RE, relative expression. Data are expressed as means ± SEM from three independent experiments. *P* values were calculated using Student's *t* test. *, $P < 0.05$; **, $P < 0.01$; ***, $P < 0.001$.

SL2 were observed in pseudoknot regions of HENXX-8, HNjz15, IAF-exp91, HENXX-1, HNhx, FJWQ16, FJXS15, FJZ03, and Prime Pac strains, which might confer more stable base pairing (bases marked with black lines). For EAV, most strains were identical to the Bucyrus standard isolate, but Vienna, CW01, and F27 strains contained one or two nucleotide changes. Taken together, the sequence alignments revealed that the pseu-

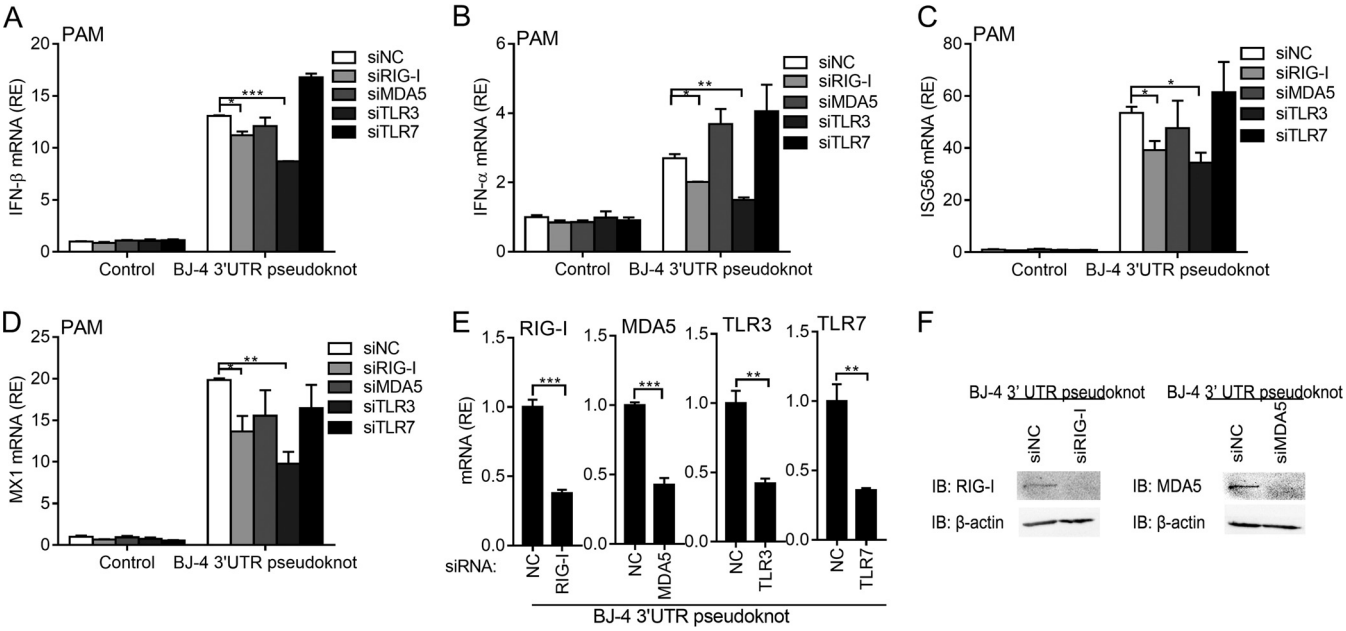

FIG 6 Recognition of the pseudoknot of PRRSV 3′ UTR is mediated by RIG-I and TLR3. (A to D) PAMs were treated with 20 nM control siRNA (siNC) or siRNA against RIG-I, MDA5, TLR3, and TLR7 and then transfected with BJ-4 3′ UTR pseudoknot or the no-RNA control for 6 h, and the IFN-β, IFN-α, ISG56, and MX1 mRNA levels were analyzed by qRT-PCR. (E and F) To ensure knockdown efficiency, RIG-I, MDA5, TLR3, and TLR7 mRNA levels were analyzed by qRT-PCR and IB. RE, relative expression. Data are expressed as means ± SEM from three independent experiments. *P* values were calculated using Student's *t* test. *, $P < 0.05$; **, $P < 0.01$; ***, $P < 0.001$.

doknot sequences were conserved in different arteriviruses. After alignment, we further extended our research to predict the RNA secondary structure of the 3′ terminus region of the arterivirus genomes using Mfold software based on previous studies (58) (Fig. 9B). The predicted results showed that other arterivirus members, including EAV, LDV, and SHFV, possessed pseudoknot structure. Moreover, previous reports obtained evidence of the pseudoknot interaction near the 3′ end of the EAV genome (58). We next investigated the IFN stimulatory activity of the pseudoknot in all known arteriviruses. The predicted pseudoknot regions residing in the 3′ UTR of EAV, PRRSV, LDV, or SHFV were generated and transfected into PAMs for 6 h. The results indicated that all predicted pseudoknot regions of EAV, PRRSV, LDV, and SHFV induced IFN-β and IFN-α mRNA increase (Fig. 9C). We then further ensured that the pseudoknot interaction was crucial for IFN induction. We conducted a series of mutants of the pseudoknot of the EAV 3′ UTR using a mutation strategy similar to that used for PRRSV strain BJ-4 (58). The pseudoknot interaction was disrupted without affecting the predicted structure of the unique hairpins. In mutants OR4 and OR5, the orientations of the central pentanucleotide sequences in the SL4 and SL5 loops were changed. In mutants SW4 and SW5, the central five nucleotides in the SL4 and SL5 loops were switched. Double mutants OR45 and SW45 were generated to restore the base-pairing possibilities. These mutants then were transfected into PAMs for 6 h or 12 h. As expected, OR45 and SW45 showed the highest IFN-β and IFN-α mRNA responses, similar to those of the original pseudoknot of EAV (Fig. 9D). The mutants SW4, SW5, OR4, and OR5 exhibited lower IFN induction than the original pseudoknot of EAV. Taken together, these results strongly demonstrated that the pseudoknot interaction was important for IFN induction, which was conserved among arteriviruses.

DISCUSSION

In the present study, we confirmed that PRRSV induced IFN and IFN-stimulated gene production in CRL-2843 cells and PAMs (Fig. 1), in line with previous studies (47, 48). The host PRRs RIG-I, TLR3, and MDA5 were all involved in the IFN induction by PRRSV (Fig. 2). We next identified an RNA pseudoknot structure residing in the PRRSV 3′ UTR

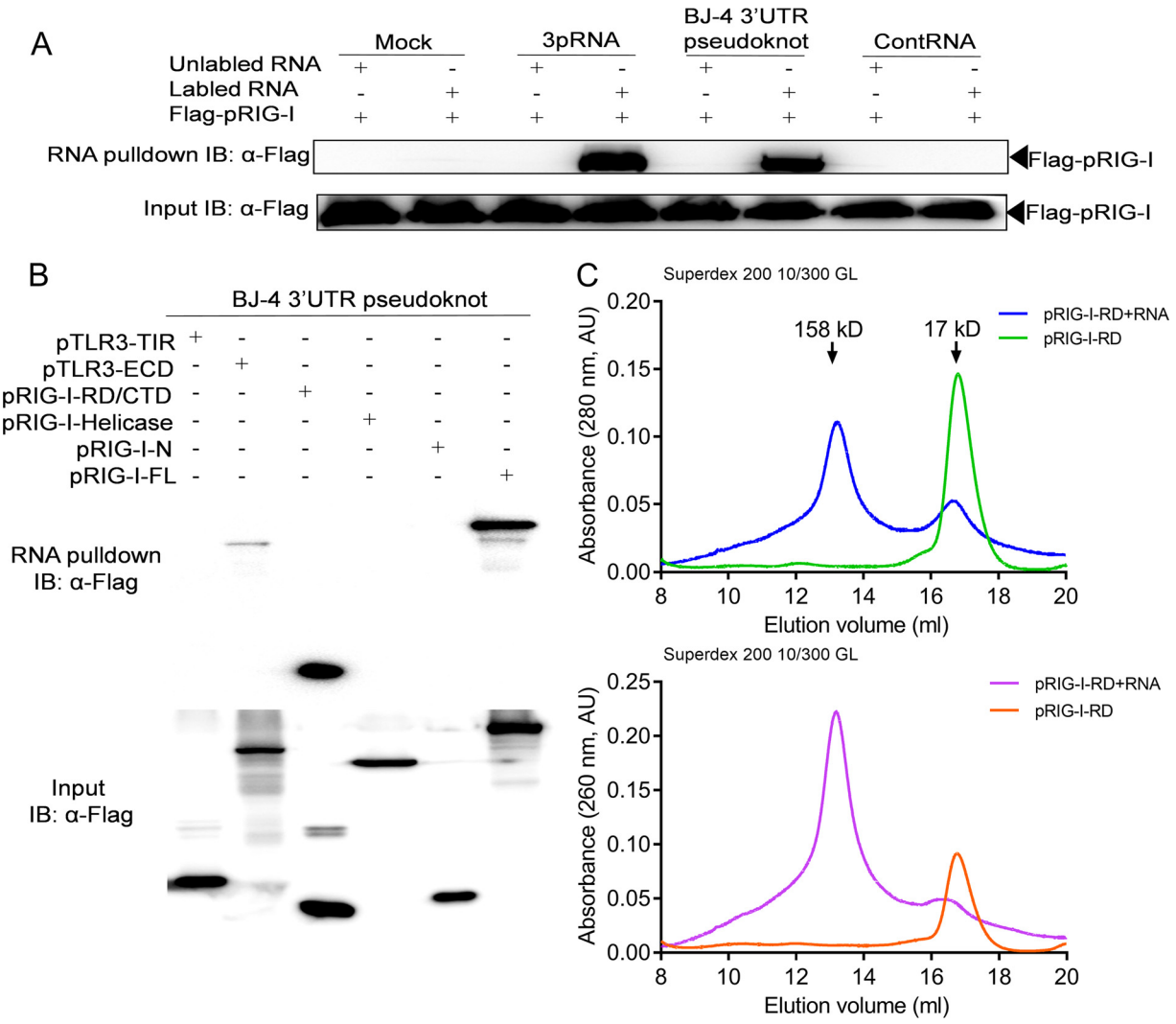

FIG 7 RIG-I and TLR3 interact with the pseudoknot of PRRSV 3′ UTR. (A and B) RNA pulldown assay showing the binding activity of the indicated RNAs to Flag-pRIG-I in HEK293T cells. (A) The HEK293T cell lysates overexpressing Flag-pRIG-I were incubated with unlabeled or biotinylated BJ-4 3′ UTR pseudoknot transcripts, negative capped-RNA control (ContRNA), or 3pRNA (a RIG-I ligand as positive control). After streptavidin bead pulldown, the bound proteins were analyzed by WB with anti-Flag MAb. (B) The HEK293T cell lysates overexpressing Flag-pRIG-I- or Flag-pTLR3-truncated mutants were incubated with biotinylated 3′ UTR pseudoknot transcripts. After streptavidin bead pulldown, the bound proteins were analyzed by IB with anti-Flag MAb. (C) Binding analysis of pRIG-I-RD and BJ-4 3′ UTR pseudoknot transcripts by gel filtration chromatography. The pRIG-I-RD and BJ-4 3′ UTR pseudoknot transcript chromatograms were mixed at a 2:1 molar ratio on ice for 1 h. Plotted are UV absorption profiles (260 nm and 280 nm). The retention volumes for each elution are shown on the chromatograms.

that served as a PAMP and was directly involved in IFN induction (Fig. 4). Conversely, disruption of loop interaction inside the pseudoknot by introducing nucleotide mutation impaired IFN production (Fig. 5). Our data demonstrated that the sensing of the pseudoknot was mediated by RIG-I and TLR3 (Fig. 6 and 7). Interestingly, the *in silico* prediction analysis indicated the structure of EAV, LDV, and SHFV near the 3′ end possessed similar pseudoknot interaction, which was conserved within arterivirus genomes (58) and contributed to mediating the similar IFN response (Fig. 9). More importantly, we found that transfection of the wild-type pseudoknot, but not the mutants, significantly inhibited PRRSV replication (Fig. 8). These results clearly demonstrated that the pseudoknot residing in the 3′ UTR was significant to stimulation of RIG-I and TLR3-mediated signaling pathways and provoking an antiviral response.

PRRSV possesses extremely complex RNA virus replication mechanisms using many noncanonical translational strategies, one of which is subgenomic mRNA synthesis (64). Thus, during PRRSV infection and replication, numerous forms of nucleic acids, includ-

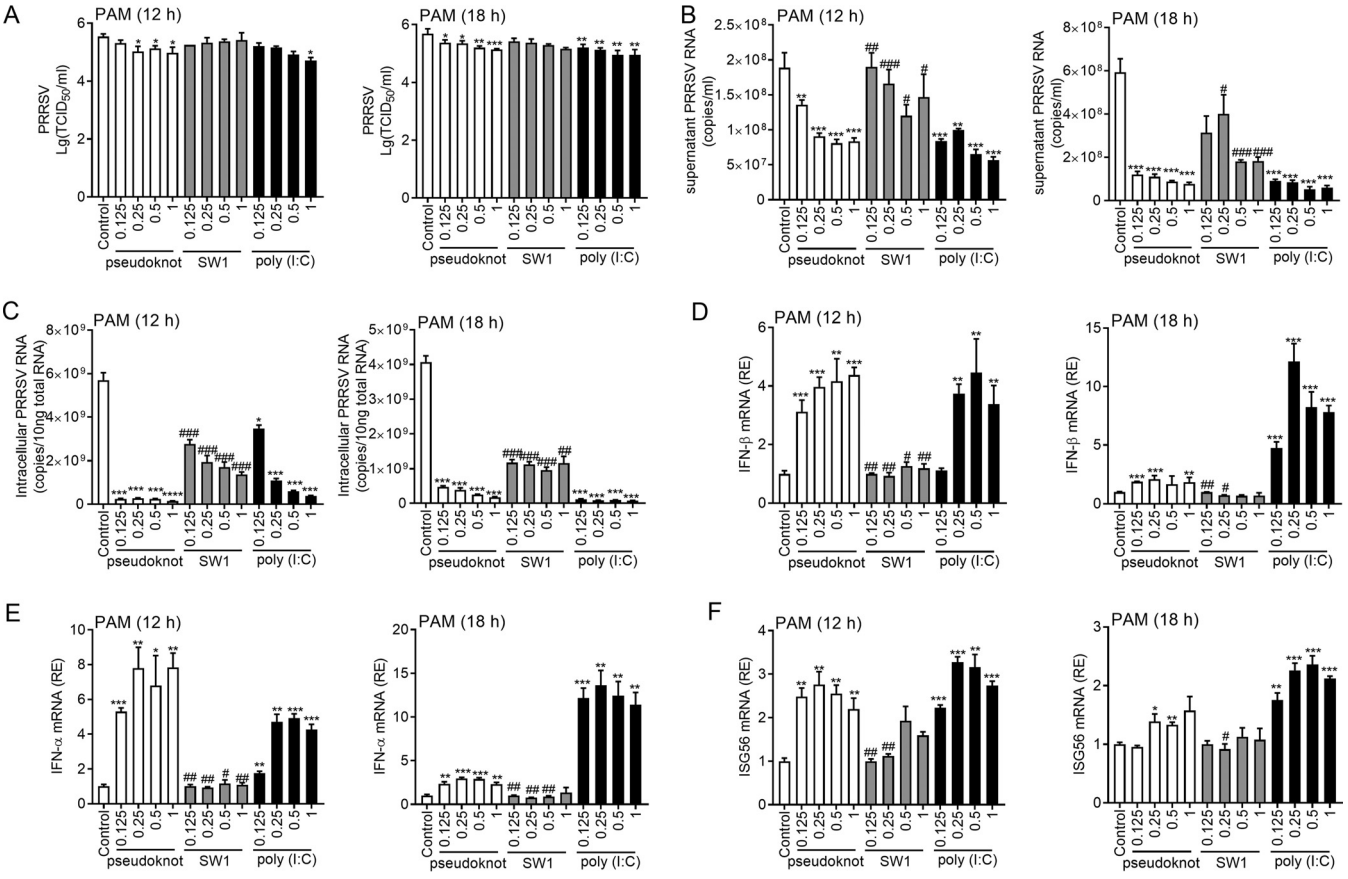

FIG 8 BJ-4 3′ UTR pseudoknot transcripts restrict PRRSV replication in PAMs. (A, B, and C) PAMs were transfected with BJ-4 3′ UTR pseudoknots, BJ-4 3′ UTR pseudoknot SW1 transcripts, 1 μg poly(I·C), or no-RNA control, respectively. Cells then were infected with PRRSV BJ-4 for 12 h or 18 h. The supernatants were collected for $TCID_{50}$ determination (A) and analysis of copy numbers of PRRSV (B). (C) Cells were collected for the PRRSV detection by qRT-PCR. (D, E, and F) PAMs were transfected with BJ-4 3′ UTR pseudoknot, BJ-4 3′ UTR pseudoknot SW1 transcripts, 1 μg poly(I·C), or no-RNA control. Cells then were infected with PRRSV BJ-4 for 12 or 18 h, and IFN-β, IFN-α, and ISG56 were analyzed by qRT-PCR. RE, relative expression. Data are expressed as means ± SEM from three independent experiments. Statistical analysis was performed by Student's *t* test. *, $P < 0.05$; **, $P < 0.01$; ***, $P < 0.001$ [for 50-151 WT or poly(I·C) compared to control]; #, $P < 0.05$; ##, $P < 0.01$; ###, $P < 0.001$ (for BJ-4 3′ UTR pseudoknot SW1 compared to BJ-4 3′ UTR pseudoknot).

ing positive-sense ssRNA, negative-sense ssRNA, and dsRNA, coexist in cells. We speculated that the recognition of PRRSV was correspondingly complicated. We first analyzed whether the 5′ UTR and 3′ UTR had IFN-inducing effects. The results showed that both the full-length 5′ UTR and 3′ UTR increased IFN-β and IFN-α production with a dose-dependent effect (Fig. 3). To determine the exact region required for IFN induction, we predicted the secondary structure of 5′ UTR and 3′ UTR by Mfold software and synthesized full-length and truncated RNA using the *in vitro* transcription system or chemical synthesis to assess the IFN response of the 5′ UTR and 3′ UTR. Unexpectedly, none of the truncated segments showed the remarkable IFN response (Fig. 3). Interestingly, we found the alternative structure of the PRRSV 3′ UTR pseudoknot structure involved in PRRSV replication was responsible for IFN induction (Fig. 4). This is in concert with IFN induction by the whole virus, which is related to PRRSV replication (Fig. 1F). Previous studies have demonstrated that the subgenomic RNAs of *Nidovirales* viruses generate a nested 3′-coterminal set of subgenomic mRNAs, and genome replication and single guide RNA (sgRNA) synthesis are initiated at the 3′ end of the viral genome RNA (65–67). Thus, the IFN stimulatory activities of the pseudoknot structures of the 3′ end might possess general significance. The RNA synthesis process of viruses in *Nidovirales* can be controlled via RNA structure conformational switches. The pseudoknot structure in the PRRSV 3′ UTR has been suggested to have an important regulatory effect on viral genome replication, sgRNA transcription, and viability (58). The conformational switches in replication possibly benefit virus recog-

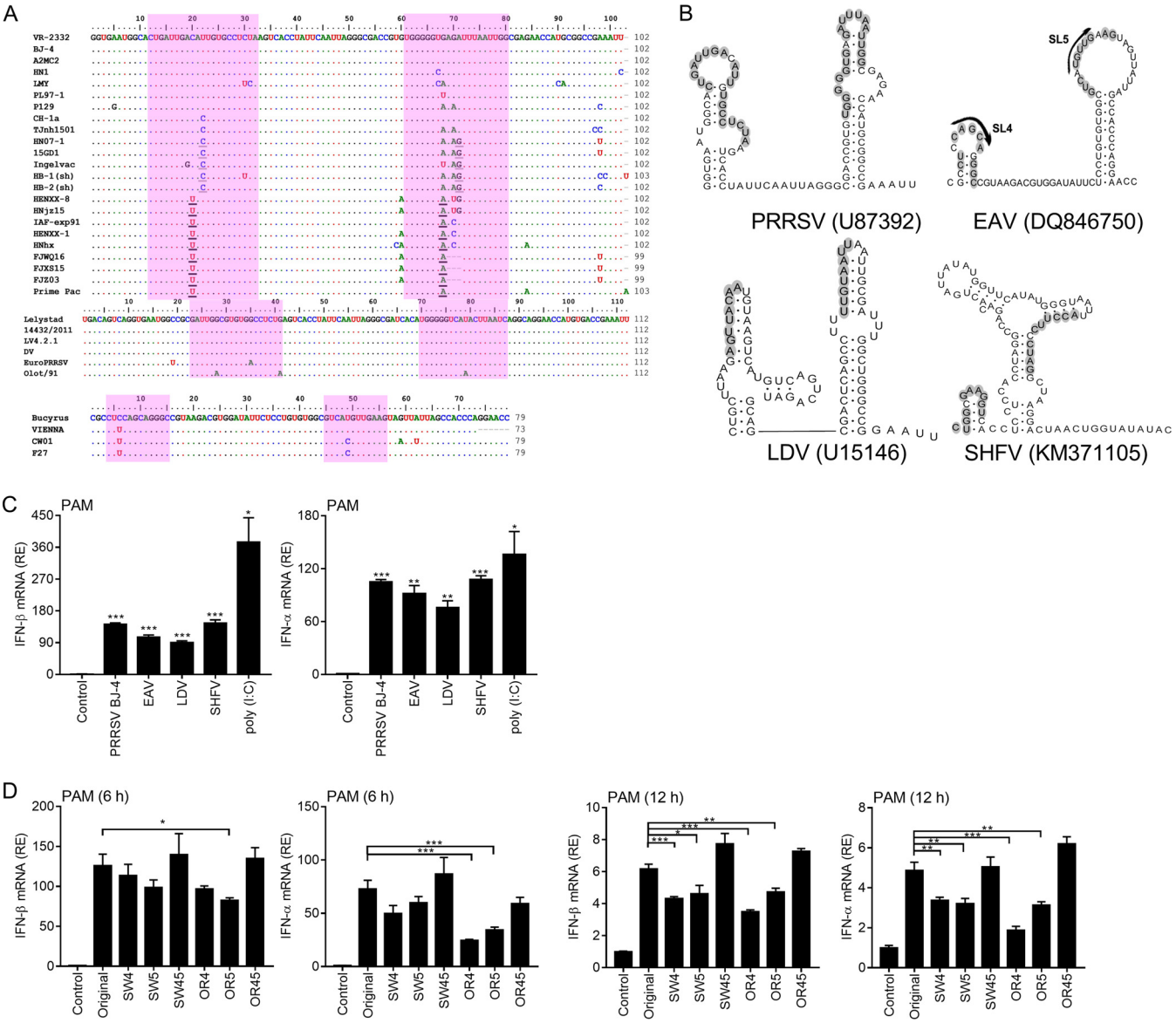

FIG 9 IFN stimulatory activity of the pseudoknot is conserved in all known arteriviruses. (A) Alignment of the nucleotides involved in the pseudoknot interaction in different members of arteriviruses. Pseudoknot interaction was represented in pink regions using BioEdit. The covarying base changes within pseudoknots were discriminatively underlined. The sequence and accession numbers used here are the following: for PRRSV type 2 (North American type), the isolates were VR2332 (U87392), BJ-4 (AF331831), A2MC2 (JQ087873), HN1 (AY457635), LMY (DQ473474), HN07-1 (KX766378), 15GD1 (KX815407), P129 (AF494042), CH-1a (AY032626), PL97-1 (AY585241), TJnh1501 (KX510269), Ingelvac (DQ988080), HB-1 (sh) (AY150312), HB-2 (sh) (AY262352), FJZ03 (KP860909), HENXX-1 (KU950372), HNhx (KX766379), HNjz15 (KT945017), IAF-exp91 (U02095), FJWQ16 (KX758249), FJXS15 (KX758250), HENXX-8 (KY041782), and Prime Pac (DQ779791); for PRRSV type 1 (European type), the isolates shown were Lelystad (M96262), 14432/2011 (KR296711), LV4.2.1 (AY588319), DV (KF991509), EuroPRRSV (AY366525), and Olot/91 (X92942); for EAV, the isolates shown were Bucyrus (NC_002532), Vienna (X78497), CW01 (AY349168), and F27 (JN211316). (B) The RNA secondary structure predictions in different arterivirus genomes for the possible pseudoknot interaction between the terminal hairpin and the upstream hairpin are shown and marked in gray. The predicted pseudoknot of EAV (Brucyrus [accession number DQ846750]), SHFV (M6941 [accession number KM371105]), LDV (Plagemann [accession number U15146]), and PRRSV (VR2332 [accession number U87392]) are shown. (C) Analysis of the IFN stimulatory activity of PRRSV, EAV, LDV, and SHFV. PAMs were transfected with the pseudoknot of PRRSV, EAV, LDV, and SHFV genome constructs, 1 μg poly(I·C), or no-RNA control for 6 h, and the IFN-β and IFN-α mRNA levels were analyzed by qRT-PCR. (D) PAMs were transfected with original or mutant pseudoknot transcripts of EAV (SW4, SW5, SW45, OR4, OR5, and OR45) or no-RNA control for 6 h or 12 h, and the IFN-β and IFN-α mRNA levels were analyzed by qRT-PCR. RE, relative expression. Data are expressed as means ± SEM from three independent experiments. *P* values were calculated using Student's *t* test. *, $P < 0.05$; **, $P < 0.01$; ***, $P < 0.001$.

nition. More importantly, the similar pseudoknot structures among other arterivirus members were also sufficient for IFN production (Fig. 9).

Although SL1/SL2 without interaction are likely to be more stable than the pseudoknot, a great deal of evidence has shown that the pseudoknot interaction can be formed from transfected 3′ UTR RNA. (i) Previous studies showed that the infectious

progeny can be successfully detected in cells transfected with EAV RNA (obtained by *in vitro* transcription) without viral component cotransfection, suggesting that the pseudoknot which is necessary for replication can be formed in the absence of other viral components (58, 68). (ii) Studies on bovine coronavirus obtained enzymatic probing evidence for the existence of the pseudoknot of synthetic transcripts (69). (iii) Experiments suggested that the formation and stability of pseudoknots are involved in the sequence and size of the loop regions, temperature, and ionic conditions, such as the presence of Mg^{2+} (70). Thus, the pseudoknot fragments used in this study were synthesized by *in vitro* transcription in our study. Indeed, our study demonstrated that the SL1/SL2 or SL4/SL5 mutant segments which disrupted the pseudoknot interaction dramatically dampened IFN induction compared to that of the original pseudoknot RNA, while OR12/SW12 mutants of PRRSV (or SL45/SW45 in EAV), which restored base pairing, induced IFN response as efficiently as the wild type. These results strongly suggested that the pseudoknot interaction was formed from the *in vitro*-transfected 3′ UTR RNA (Fig. 5 and 9D). Despite all this, the exact pieces of evidence need to be obtained through methods such as three-dimensional modeling and structural determination.

PRRSV is characteristic of immunosuppression and persistent infection. Previous studies have demonstrated that PRRSV induced weaker responses than sensitive IFN agonists, such as TGEV or poly(I·C) (43, 44). Thus, most reports have placed emphasis on how PRRSV evades host immune responses. For instance, PRRSV interferes with the activation and signaling pathways of IFNs, such as by blocking ISG factor 3 (ISGF3) nuclear translocation or blocking STAT1/STAT2 nuclear translocation (71–73). Viral nonstructural proteins (nsp1, -2, -4, -11) and a structural protein (N) have been shown to downregulate IFN through interacting with RLR andTLR signaling pathways (71–77), which probably enable PRRSV to escape from antiviral innate immune response. However, type I IFN is important for antiviral response and inhibiting PRRSV infection, which has been demonstrated *in vitro* and *in vivo* (45, 46, 78, 79). Recognition of viruses is the initiation of antiviral immune response. Here, we observed robust induction of IFN by an RNA pseudoknot region, including IFN-β and IFN-α (Fig. 4). This suggested that PRRSV components indeed have its ability to induce antiviral signaling, whereas the proteins of PRRSV, especially nsps, inhibit host antiviral immune responses. We also observed IFN-β, IFN-α, IFN-γ, and ISG induction by live virus. The induction was abolished by virus inactivation, indicating that virus replication is required for IFN induction (Fig. 1). This is consistent with the function of pseudoknot on viral RNA synthesis. However, the conventional type II strain (represented by BJ-4) and HP-PRRSV (represented by HN07-1) showed a discrepant response on IFN or ISG induction. This strain-dependent effect needs to be studied further. Moreover, transfection of the pseudoknot segment suppressed PRRSV replication in PAMs, which was consistent with the effects of the induction of innate immunity (Fig. 8). However, there is a possibility that the transfected pseudoknot fragment acts as a competitive inhibitor through titration of viral protein and RNA components that normally interact with the 3′ UTR during infection. Previous studies showed that (i) the pseudoknot could be recognized by the viral replicase complex elements to control the arterivirus RNA synthesis (58), and (ii) the upstream stem-loop (SL1) in the 3′ UTR pseudoknot could interact with a hairpin located in the N protein gene to form a "kissing loop interaction" which is also essential for RNA replication (80). Thus, the transfected pseudoknot RNA might competitively bind with viral replicase complex or other elements seated in the end of the virus genome to affect virus RNA synthesis.

Among PRRs, TLRs and RLRs recognize distinct types of nucleic acids during viral infection. RIG-I senses RNA with uncapped 5′-triphosphates (81), base-paired structures, or panhandle structures (33, 36). As for dsRNA recognition, its length decides the differential recognition by RIG-I and MDA5. RIG-I senses short dsRNAs, whereas MDA5 senses long dsRNAs (36, 82). Moreover, recognition mechanisms vary greatly depending on cell types (83). TLRs are dispensable for IFN induction, except in the case of plasmacytoid dendritic cells (pDCs) (83). Recent research reveals that MDA5 senses the EAV genome to induce IFN expression (84). There also have been several reports

showing that PRRSV could cause the immune response despite the fact that the response is weak (73). We identified that RIG-I, MDA5, and TLR3 were all involved in IFN induction (Fig. 2). We speculate that this is correlated with the existence of numerous forms of nucleic acids due to the complicated replication mechanism of PRRSV. The pseudoknot recognition depended on RIG-I and TLR3, which was verified by direct interaction of the pseudoknot structure using RNA pulldown (Fig. 7). Furthermore, RNA pulldown indicated that the RD domain showed strong binding ability with the pseudoknot. Coincidently, previous studies on the crystal structure of RIG-I revealed that it is the RD domain of RIG-I which binds with 5′ppp dsRNA (81, 85), and Devarkar et al. demonstrated the interaction of the helicase-RD domain with Cap-0 dsRNA as well as 5′ppp RNA through determining the structures of the complexes (86). Therefore, the RD domain of RIG-I is crucial for RNA recognition.

The PRRSV genome was deemed to possess a 5′ cap structure. The cap structure contains three cap types, cap-0, cap-1, and cap-2, depending on the position of 2′-*O*-methyl modification. However, the cap-0 structure's formation requires 3 sequential reactions catalyzed by RNA triphosphatase (TPase), guanylyltransferase (GTase), and (guanine-N7)-methyltransferase (N7-MTase) (87). In higher eukaryotes or most viruses, to form a cap-1 structure, the cap-0 structure is further methylated at the first nucleotide of the ribose 2′-*O* position via ribose 2′-*O*-methyltransferase (2′-*O*-MTase). However, arteriviruses inclusive of PRRSV do not encode 2′-*O*-MTase according to bioinformatic analysis and MTase assay (88). Thus, the type of 5′ cap structure of PRRSV is unclear. The adding cap type in our study is cap-0. Previous studies have shown that m7G, which hinders RIG-I binding, is essential for distinction between self and nonself RNA. However, recent research shows that m7G dsRNA, as well as 5′ppp dsRNA, has RIG-I binding activity (86). Thus, the cap contribution in PRRSV sensing needs more studies.

We proposed a model on the balance between the stimulatory effect of the 3′ pseudoknot structure and the downregulation by the viral proteins (Fig. 10). At the early endosomes, the viral genome is released into the cytoplasm. The genomic RNA serves as the mRNA for immediate translation of the large replicase polyproteins, pp1a and pp1ab. After cleavage, these proteins assemble into a replication and transcription complex (RTC). The RTC immediately binds 3′ UTR to initiate minus-strand RNA synthesis. During this replication, the pseudoknot of the genome is recognized by RNA sensor RIG-I through its RD domain and TLR3 through its ectodomain (ECD), resulting in IRF3 or NF-κB activation and triggering IFN gene expression. The generated viral proteins, such as nsp1/2/4/11 and N protein, affect the host antiviral response by targeting signaling pathways, such as IRF3, NF-κB, and ISGF3. During this process, the conformational change of the 3′ end, which acts as a molecular switch to regulate the timing of viral synthesis, might affect virus recognition and subsequent IFN response.

In summary, we characterized the pseudoknot structure of PRRSV and other members of arteriviruses regarding the nature of immune recognition of PAMPs. In addition, the pseudoknot of PRRSV activated antiviral signaling via interaction with RIG-I and TLR3. These results will contribute to our understanding of PRRSV pathogenicity and the development of antiviral strategies.

MATERIALS AND METHODS

Cells and viruses. Cell cultures and all incubations or reactions were performed at 37°C in a humidified atmosphere of 5% CO_2 according to the manufacturers' instructions, unless otherwise specified. The PAM cell lines CRL2843 (3D4/21) and CRL2843-CD163, a cell line stably expressing CD163 in CRL2843 (89), were maintained in RPMI 1640 medium supplemented with 10% fetal bovine serum (FBS; Gibco), 100 U/ml penicillin, and 100 μg/ml streptomycin as described previously. Marc-145 cells were maintained in Dulbecco's modified Eagle's medium (DMEM) with 10% FBS, 100 U/ml penicillin, and 100 μg/ml streptomycin. PAMs were prepared from lung lavage of 4- to 6-week-old specific-pathogen-free (SPF) piglets (90) and maintained in RPMI 1640 with 10% heat-inactivated FBS and penicillin-streptomycin. HN07-1 (GenBank accession number KX766378.1) was isolated by our laboratory during HP-PRRSV outbreaks in 2007 and proven to be a highly pathogenic PRRSV (HP-PRRSV) strain by subsequent animal experiment. BJ-4 (GenBank accession number AF331831), characterized as a low-pathogenicity PRRSV strain, was a kind gift from Hanchun Yang (China Agricultural University). These PRRSV strains were propagated and titrated on Marc-145 cells and stored at −80°C. The UV-inactivated

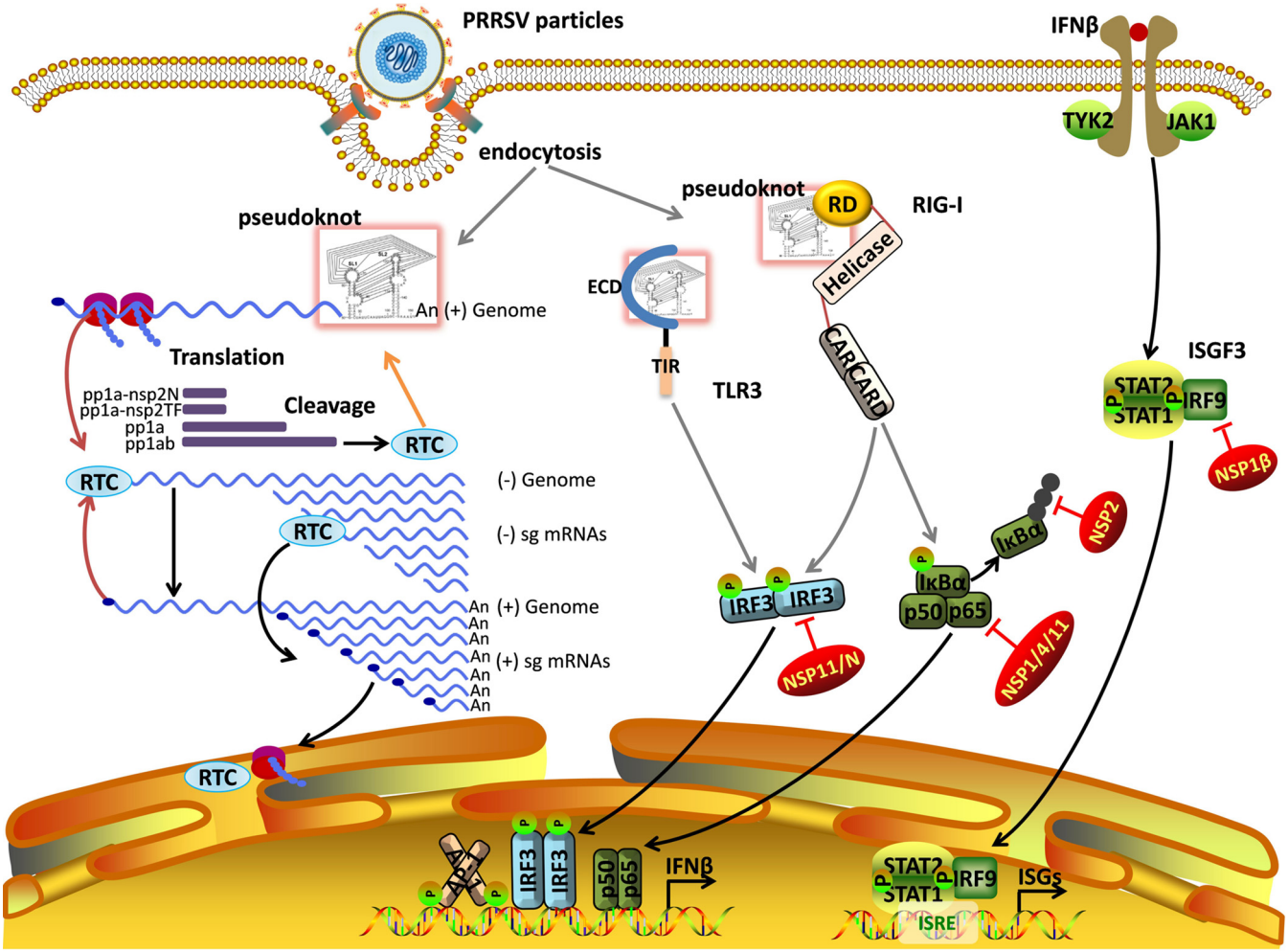

FIG 10 Balance between the immune recognition role by the pseudoknot within the PRRSV life cycle and the immunosuppression phenotype by PRRSV protein.

PRRSV was prepared via exposure to UV irradiation (254 nm) of live PRRSV for 2 h. Heat inactivation of PRRSV was performed by water bath at 65°C for 30 min.

Plasmid construction. To construct plasmids expressing Flag-tagged *Sus scrofa* RIG-I and TLR3 (Flag-pRIG-I and Flag-pTLR3), the cDNA fragments carrying the ORF of these genes were obtained by reverse transcription-PCR (RT-PCR) using RNA extracted from CRL2843-CD163 cells as templates and inserted into pEF-BOS vector. Truncated mutants of RIG-I and TLR3 were generated based on Flag-pRIG-I and Flag-pTLR3 plasmids. IFN-β-luciferase reporter (IFN-β-Luc) vector was constructed by inserting the promoter region of the *Sus scrofa* IFN-β gene (-296 to $+52$) into pGL4.17 vector (Promega). T7 promoter-driven RNA expression vectors, designated pMD19T-5′ UTR and pMD19T-3′ UTR, were constructed for *in vitro* transcription. The full-length 5′ UTR and 3′ UTR cDNA sequences were amplified by RT-PCR using RNA extracted from PRRSV BJ-4-infected PAMs and subcloned into pMD19T-simple vector. All primers used are listed in Table 1.

Antibodies and reagents. Rabbit anti-RIG-I (D33H10), anti-actin (13E5), and anti-MDA5 (D74E4) antibodies were purchased from Cell Signaling Technology (CST). Mouse anti-Flag (M2) antibody was purchased from Sigma-Aldrich. Horseradish peroxidase (HRP)-conjugated anti-mouse IgG and anti-rabbit IgG (Jackson ImmunoResearch) were used as secondary antibodies at a dilution of 1:5,000. Polyinosinic-poly(C) [poly(I·C)] was purchased from Sigma-Aldrich.

Immunoblotting. Cells were harvested and lysed in immunoprecipitation (IP) lysis buffer (Pierce) supplemented with protease and phosphatase inhibitors. Protein samples were separated by SDS-PAGE and transferred onto polyvinylidene difluoride (PVDF) membranes (Merck Millipore). After blocking for 1 h in 5% skim milk, the membranes were incubated with the indicated primary specific antibodies diluted to the following levels: anti-RIG-I, 1:1,000; anti-MDA5, 1:1,000; anti-actin, 1:1000; and anti-Flag, 1:1,000. The membranes then were probed with HRP-conjugated anti-rabbit or anti-mouse IgG, and immunoreactive bands were visualized with enhanced chemiluminescence (ECL) reagent (CST) according to the manufacturer's instructions.

RNA isolation and qRT-PCR. Total RNAs were isolated from CRL2843-CD163 and PAMs using TRIzol reagent (Invitrogen) by following the manufacturer's instructions. cDNA was prepared from total RNAs

TABLE 1 Sequences of primers used for vector construction or PCR amplification

Name	Sequence (5′–3′)
pRIG-I (1-943aa)	Sense, AGGATGATGATGATAAAGGTACAGCAGAGCAGCGGCGG Antisense, TGAAGATTGAGGACCTGATATCACTCAAGGTTGCCCATTCC
pRIG-I-N (1-172aa)	Sense, AGGATGATGATGATAAAGGTATGACAGCAGAGCAGCGG Antisense, TGAAGATTGAGGACCTGATATCATTTCAAAGTTTTAGGCCAATTCTC
pRIG-I-helicase (249-779aa)	Sense, AGGATGATGATGATAAAGGTCTTGCTTTACCTGCTCAG Antisense, TGAAGATTGAGGACCTGATATCATACTGCTTCATCCCATG
pRIG-I-RD (795-928aa)	Sense, AGGATGATGATGATAAAGGTAGGGATAATCAAGGAAAACCAG Antisense, TGAAGATTGAGGACCTGATATCAGGCCATTTCTGCAGC
pTLR3-TIR (27-703aa)	Sense, GCTCTAGATAAGCCACCATGGATTATAAGGATGATGATGATAAAGGTGATTATAAGGATGAT GATGATAAAGGTAACAAATGTACTGTTAGACATGAAATAGC Antisense, GGGGTACCTCAAAATGGGGCACTGTCTTTGCA
pTLR3-ECD (727-905aa)	Sense, GCTCTAGATAAGCCACCATGGATTATAAGGATGATGATGATAAAGGTGATTATAAGGATGAT GATGATAAAGGTGAAGGCTGGCGGATATCTTTTTATTGG Antisense, GGGGTACCTTAATGTACTGAATTTCTGGAACCAAGTGC
5′ UTR	Sense, TAATACGACTCACTATAGGGTATGACGTATAGGTGTTGG Antisense,[a] GGTTAAAGGGGTGGAGAGA
3′ UTR	Sense, TAATACGACTCACTATAGGGTGGGCTGGCATTCTTGAGGCAT Antisense,[a] AATTTCGGCCGCATGGTT
IFN-β promoter	Sense, GGCGGTACCCTTGGCTTATGGTGGTTTTTTTTG Antisense, TTTCTCGAGGCTCCACTACTCAAGTGCTGAAG

[a]The first two nucleotides of the antisense 5′ termini were modified with 2-*O*-Me (2′-*O*-methyl).

using a PrimeScript RT reagent kit with gDNA Eraser (TaKaRa). Quantitative RT-PCR was performed using a FastStart Universal SYBR green master (ROX) kit (Roche) on a 7500 Fast real-time PCR system (Applied Biosystems). Relative analysis of gene expression was evaluated using the $2^{-\Delta\Delta CT}$ method (91), and glyceraldehyde-3-phosphate dehydrogenase (GAPDH) mRNA was set up as an endogenous control. For detection of PRRSV RNA copies in cell supernatant, absolute quantitative PCR was performed as described previously using primers designed against PRRSV ORF7 (92). Briefly, a plasmid bearing a fragment of the PRRSV ORF7 sequence (372 bp) was constructed to generate a standard curve, and then PRRSV RNA copies in all samples were calculated by normalization to the standard curve. Gene-specific primers for pig IFN-β, IFN-α, IFN-γ, IFN-λ1, PKR, OAS, ISG56, MX1, DDX58 (RIG-I), MDA5, TLR3, TLR7, PRRSV ORF7, and GAPDH are listed in Table 2.

siRNA-mediated gene silencing and transfection. The siRNAs targeting RIG-I, MDA5, TLR3, TLR7, and negative-control siRNA (NC) were designed and synthesized by GenePharma (Table 3). CRL2843-CD163 or PAMs were transfected with siRIG-I, siMDA5, siTLR3, siTLR7, or siNC (as a negative control) using Lipofectamine RNAiMAX (Invitrogen). After transfection for 24 h, cells were infected with PRRSV for 12 h to 36 h or transfected with prepared RNA for 6 h, and then cells were harvested for subsequent mRNA or protein expression analysis.

TABLE 2 Sequences of primers used for qRT-PCR

Name	Forward (5′→3′)	Reverse (5′→3′)
IFN-β	TGCAACCACCACAATTCC	CTGAGAATGCCGAAGATCTG
IFN-α	GCCTCCTGCACCAGTTCTACA	TGCATGACACAGGCTTCCA
IFN-γ	AATGGTAGCTCTGGGAAACTG	ACTTCTCTTCCGCTTTCTTAGG
IFN-λ1	GGTGCTGGCGACTGTGATG	GATTGGAACTGGCCCATGTG
PKR	AAAGCGGACAAGTCGAAAGG	TCCACTTCATTTCCATAGTCTTCTGA
OAS	GAGCTGCAGCGAGACTTCCT	TGCTTGACAAGGCGGATGA
ISG56	TCAGAGGTGAGAAGGCTGGT	GCTTCCTGCAAGTGTCCTTC
MX1	GGCGTGGGAATCAGTCATG	AGGAAGGTCTATGAGGGTCAGATCT
DDX58 (*RIG-I*)	TATGTGCTCCTACTGGTTGTGGAAA	AGTTGAATAGCAAAAAAGACAACCT
MDA5	CTTCTGGTTACCGATGTCTTGG	CTCCCTTACTCCTGATTCATTTCC
TLR3	CATTGAGAATCTATCCCTGAGCAA	TGAGGTTTGTCTGCTTTAGTCCAA
TLR7	AAACTCTGCCCTGTGATGTCAGT	GAATCGCTGTCAAGTGCTTGTC
PRRSV ORF7	AAACCAGTCCAGAGGCAAGG	GCAAACTAAACTCCACAGTGTAA
GAPDH	CCTTCCGTGTCCCTACTGCCAAC	GACGCCTGCTTCACCACCTTCT

TABLE 3 siRNA sequences

Target gene	Target sequence (5′→3′)
DDX58 (*RIG-I*)	GCAGGUUAUUCUGGACUUUTT
MDA5	CCUCAGAUAUUGGGACUAATT
TLR3	GCUUAAGUGUGAUUGGUAATT
TLR7	CCUUGGACCUAAGUAGAAATT

Luciferase reporter assay. CRL2843-CD163 or Marc145 cells were transiently transfected with 1 μg IFN-β-Luc and 100 ng pRL-TK renilla luciferase reporter plasmid (Promega) as an internal control, and then cells were inoculated with PRRSV at 24 h or transfected with 1 μg full-length 3′ UTR or truncated fragments, including 1-151, 50-88, or pseudoknot fragment of the 3′ UTR, using TransMessenger (Qiagen). After infection with PRRSV for 24 h or transfection with RNA segments for 6, 12, and 24 h, cells were lysed and luciferase activities were measured with the Dual-Luciferase reporter assay system (Promega) according to the manufacturer's instructions.

RNA preparation and transfection. 3pRNA (5′-triphosphate RNA) and ContRNA were used as RIG-I ligand and negative capped-RNA control, respectively, and were obtained as previously described, with minor modifications (34, 54). 3pRNA was *in vitro* transcribed by a T7 polymerase using annealed complementary oligonucleotides as substrates with MEGAshortscript (Ambion) (Table 4) and was used for transfection at 1 μg (34). ContRNA samples were prepared by *in vitro* transcription using annealed oligonucleotides containing T7 promoter as templates (Table 4) with the mMESSAGE mMACHINE kit (Ambion). 2-*O*-Methylation of the first two nucleotides at the antisense 5′ terminus was conducted to prevent the nucleotide adding to the 3′ terminus of transcribed RNAs (52). In order to check the integrity of *in vitro*-transcribed RNAs, urea denaturing gel electrophoresis was conducted. As for RNA fragments of PRRSV, 5′ UTR, 3′ UTR, and truncated RNA fragments were *in vitro* transcribed by a mMESSAGE mMACHINE kit (Ambion) in accordance with the manufacturer's instructions, using annealed complementary oligonucleotides or the PCR products amplified from pMD19T-5′ UTR or pMD19T-3′ UTR as the template. Specifically, 100 ng of PCR template was incubated for 16 h in a 20-μl reaction volume at 37°C, followed by a further incubation with 2 U of TURBO DNase for 15 min at 37°C. The transcribed RNA then was purified by Sephadex G-25 quick-spin columns (Roche), dissolved in RNase-free water, and quantitated by a NanoDrop 2000c (Thermo Scientific).

The truncated (1-49, 50-88, 89-151, 1-88, and pseudoknot) and mutant (SW12, SW1, SW2, OR12, OR1, and OR2) PRRSV or EAV 3′ UTR RNA segments were prepared by *in vitro* transcription, using a T7 polymerase and the mMESSAGE mMACHINE kit (Ambion) with annealed complementary oligonucleotides as substrates (Table 4), under the control of T7 promoter and were used for transfection at 1 μg (34). The truncated PRRSV 5′ UTR (1-49, 46-79, 71-108, 107-158, and 155-190) and 3′ UTR (1-16&131-151, 15-84, and 79-131) RNA were synthesized at GenScript and used for transfection at 1 μg or the indicated dose using TransMessenger (Qiagen) (34).

***In silico* analysis of RNA secondary structure.** The RNA secondary structure presentation in this study was predicted by the Mfold web server, version 3.2 (http://unafold.rna.albany.edu/?q=mfold/RNA-Folding-Form) (55). For analysis, the RNA secondary structures were predicted under default parameters of 37°C, 1 M NaCl, no divalent ions, and no limit on maximum distance between paired bases (55). RNAviz, version 2, was used to edit the predicted RNA secondary structures (93).

RNA pulldown. *In vitro*-transcribed RNAs described above were labeled with biotin using a Pierce RNA 3′-end desthiobiotinylation kit (Pierce). Briefly, 5 μg of nonlabeled RNA control or test RNA was labeled with biotin using T4 RNA ligase at 16°C overnight in the presence of RNase inhibitor, and then the labeled RNA was purified by chloroform-isoamyl alcohol. HEK293T cells were transfected with Flag-pRIG-I or Flag-pTLR3 and lysed with IP lysis buffer (Pierce) supplemented with protease inhibitor at 36 h posttransfection. Biotin-labeled RNA (5 μg) was incubated with Streptavidin magnetic beads. Subsequently the complex was incubated with equal amounts of lysates for 4 h with gentle shaking. Beads were washed three times. The pulldown complexes were eluted with sample buffer and analyzed by immunoblotting with the indicated antibodies.

Protein expression and purification. The cDNA encoding the RD domain of *Sus scrofa* RIG-I (residues 806 to 943) was cloned into pE-SUMO vectors (LifeSensors Inc.) and expressed in *E. coli* Transetta (DE3) cells (TransGen Biotech). Cultures were performed at 37°C, and target protein expression was induced with 0.5 mM isopropyl-β-D-thiogalactoside (IPTG) at 18°C overnight. The cells were sonicated in 20 mM Tris-HCl, pH 6.8, 150 mM NaCl, 2 mM $MgCl_2$, 4 mM dithiothreitol (DTT). The protein was purified by a His-Trap Excel (GE Healthcare) column and further purified by ion exchange using a HiTrap SP HP (GE Healthcare) column. The recovered protein then was digested, using ulp protease (Solarbio), overnight at 4°C in 20 mM Tris-HCl, pH 6.8, 500 mM NaCl, 4 mM DTT buffer. After digestion, the protein was purified using a His-Trap Excel (GE Healthcare) column. Finally, the protein was purified by gel filtration chromatography on a Superdex 200 10/300 GL column (GE Healthcare) eluted with 20 mM Tris-HCl, pH 6.8, 150 mM NaCl, 2 mM $MgCl_2$, 4 mM DTT.

RNA binding studies by gel filtration chromatography. For the RNA binding studies, the PRRSV BJ-4 3′ UTR pseudoknot RNA transcripts used to form complexes with pRIG-I-RD were generated by *in viro* transcription and purified as described above. The PRRSV strain BJ-4 3′ UTR pseudoknot RNA was mixed with the pRIG-I-RD at a molar ratio of about 2:1 on ice for 1 h, and 400-μl samples were injected over the Superdex 200 10/300 GL column (GE Healthcare) eluted with buffer (20 mM Tris-HCl, pH 6.8, 150 mM NaCl, 2 mM $MgCl_2$, 4 mM DTT). In addition, 400 μl of pRIG-I-RD protein was examined on a Superdex

TABLE 4 DNA oligonucleotides of PRRSV RNA and 3pRNA for *in vitro* transcription

Target gene	Sequence[a] (5′–3′)
3pRNA	Sense, TAATACGACTCACTATAGGGAAACTAAAAGGGAGAAGTGAAAGTG Antisense, CACTTTCACTTCTCCCTTTTAGTTTCCCTATAGTGAGTCGTATTA
ContRNA	Sense, TAATACGACTCACTATAGTTCGCAGTCCCCAACCTCCAATCACTCACCAACCTCCTGTCCTCCAATTTGTCCTGGTTTA Antisense, TAACCAGGACAAATTGGAGGACAGGAGGTTGGTGAGTGATTGGAGGTTGGGGACTGCGAACTATAGTGAGTC GTATTA
BJ-4 3′ UTR 1-49	Sense, TAATACGACTCACTATAGGGTGGGCTGGCATTCTTGAGGCATCTCAGTGTTTGAATTGGAAGAATGTGT Antisense, ACACATTCTTCCAATTCAAACACTGAGATGCCTCAAGAATGCCAGCCCACCCTATAGTGAGTCGTATTA
BJ-4 3′ UTR 50-88	Sense, TAATACGACTCACTATAGGGGGTGAATGGCACTGATTGACATTGTGCCTCTAAGTCACC Antisense, GGTGACTTAGAGGCACAATGTCAATCAGTGCCATTCACCCCCTATAGTGAGTCGTATTA
BJ-4 3′ UTR 89-151	Sense, TAATACGACTCACTATAGGGTATTCAATTAGGGCGACCGTGTGGGGGTGAGATTTAATTGGCGAGAACCATG CGGCCGAAATT Antisense, AATTTCGGCCGCATGGTTCTCGCCAATTAAATCTCACCCCCACACGGTCGCCCTAATTGAATACCCTATA GTGAGTCGTATTA
BJ-4 3′ UTR 1-88	Sense, TAATACGACTCACTATAGGGTGGGCTGGCATTCTTGAGGCATCTCAGTGTTTGAATTGGAAGAATGTGTGGT GAATGGCACTGATTGACATTGTGCCTCTAAGTCACC Antisense, GGTGACTTAGAGGCACAATGTCAATCAGTGCCATTCACCACACATTCTTCCAATTCAAACACTGAGAT GCCTCAAGAATGCCAGCCCACCCTATAGTGAGTCGTATTA
BJ-4 3′UTR pseudoknot	Sense, TAATACGACTCACTATAGGGGGTGAATGGCACTGATTGACATTGTGCCTCTAAGTCACCTATTCAATTAGGG CGACCGTGTGGGGGTGAGATTTAATTGGCGAGAACCATGCGGCCGAAATT Antisense, AATTTCGGCCGCATGGTTCTCGCCAATTAAATCTCACCCCCACACGGTCGCCCTAATTGAATAGGTGAC TTAGAGGCACAATGTCAATCAGTGCCATTCACCCCCTATAGTGAGTCGTATTA
HN07-1 3′ UTR pseudoknot	Sense, TAATACGACTCACTATAGGGGGTGAATGGCACTGATTGACACTGTGCCTCTAAGTCACCTATTCAATTAGGGC GACCGTGTGGGGGTAAAGTTTAATTGGCGAGAACCATGCGGCCGTAATT Antisense, AATTACGGCCGCATGGTTCTCGCCAATTAAACTTTACCCCCACACGGTCGCCCTAATTGAATAGGTGACT TAGAGGCACAGTGTCAATCAGTGCCATTCACCCCCTATAGTGAGTCGTATTA
BJ-4 3′ UTR pseudoknot SW12	Sense, TAATACGACTCACTATAGGGGGTGAATGGCACTTAATTGCATTGTGCCTCTAAGTCACCTATTCAATTAGGGCGAC CGTGTGGGGGTGAGATTGATTGAGCGAGAACCATGCGGCCGAAATT Antisense, AATTTCGGCCGCATGGTTCTCGCTCAATCAATCTCACCCCCACACGGTCGCCCTAATTGAATAGGTGACTTA GAGGCACAATGCAATTAAGTGCCATTCACCCCCTATAGTGAGTCGTATTA
BJ-4 3′ UTR pseudoknot SW2	Sense, TAATACGACTCACTATAGGGGGTGAATGGCACTGATTGACATTGTGCCTCTAAGTCACCTATTCAATTAGGGCGACC GTGTGGGGGTGAGATTGATTGAGCGAGAACCATGCGGCCGAAATT Antisense, AATTTCGGCCGCATGGTTCTCGCTCAATCAATCTCACCCCCACACGGTCGCCCTAATTGAATAGGTGACTTAG AGGCACAATGTCAATCAGTGCCATTCACCCCCTATAGTGAGTCGTATTA
BJ-4 3′ UTR pseudoknot SW1	Sense, TAATACGACTCACTATAGGGGGTGAATGGCACTTAATTGCATTGTGCCTCTAAGTCACCTATTCAATTAGGGC GACCGTGTGGGGGTGAGATTTAATTGGCGAGAACCATGCGGCCGAAATT Antisense, AATTTCGGCCGCATGGTTCTCGCCAATTAAATCTCACCCCCACACGGTCGCCCTAATTGAATAGGTGAC TTAGAGGCACAATGCAATTAAGTGCCATTCACCCCCTATAGTGAGTCGTATTA
BJ-4 3′ UTR pseudoknot OR12	Sense, TAATACGACTCACTATAGGGGGTGAATGGCACAGTTAGTCATTGTGCCTCTAAGTCACCTATTCAATTAGGGCGA CCGTGTGGGGGTGAGATGTTAATTGCGAGAACCATGCGGCCGAAATT Antisense, AATTTCGGCCGCATGGTTCTCGCAATTAACATCTCACCCCCACACGGTCGCCCTAATTGAATAGGTGACTTA GAGGCACAATGACTAACTGTGCCATTCACCCCCTATAGTGAGTCGTATTA
BJ-4 3′ UTR pseudoknot OR2	Sense, TAATACGACTCACTATAGGGGGTGAATGGCACTGATTGACATTGTGCCTCTAAGTCACCTATTCAATTAGGGCGAC CGTGTGGGGGTGAGATTAATTTGGCGAGAACCATGCGGCCGAAATT Antisense, AATTTCGGCCGCATGGTTCTCGCCAAATTAATCTCACCCCCACACGGTCGCCCTAATTGAATAGGTGACTTAG AGGCACAATGTCAATCAGTGCCATTCACCCCCTATAGTGAGTCGTATTA
BJ-4 3′ UTR pseudoknot OR1	Sense, TAATACGACTCACTATAGGGGGTGAATGGCACAGTTAGTCATTGTGCCTCTAAGTCACCTATTCAATTAGGGCGACC GTGTGGGGGTGAGATTTAATTGGCGAGAACCATGCGGCCGAAATT Antisense, AATTTCGGCCGCATGGTTCTCGCCAATTAAATCTCACCCCCACACGGTCGCCCTAATTGAATAGGTGACTT AGAGGCACAATGACTAACTGTGCCATTCACCCCCTATAGTGAGTCGTATTA
EAV pseudoknot	Sense, TAATACGACTCACTATAGGGCGCCTCCAGCAGGGCCGTAAGACGTGGATATTCTCCTGTGTGGCGTCATGTTGA AGTAGTTATTAGCCACCCAGGAACC

(Continued on next page)

TABLE 4 (Continued)

Target gene	Sequence[a] (5′–3′)
	Antisense, GGTTCCTGGGTGGCTAATAACTACTTCAACATGACGCCACACAGGAGAATATCCACGTCTTACGGCCCTG CTGGAGGCGCCCTATAGTGAGTCGTATTA
SHFV pseudoknot	Sense, TAATACGACTCACTATAGGGCTGGCGAAGGTCACCTCCTCCACCTAGGCCAGACACTGATTATATGGTTCATATG GGTAATTACCTTCCCTAGGCTAAGGACTAACTGGTATATAC Antisense, GTATATACCAGTTAGTCCTTAGCCTAGGGAAGGTAATTACCCATATGAACCATATAATCAGTGTCTGGCC TAGGTGGAGGAGGTGACCTTCGCCAGCCCTATAGTGAGTCGTATTA
LDV pseudoknot	Sense, TAATACGACTCACTATAGGGCTGCTTAAGAGTTACAATGTAAGTCATGTCAGTCAGATGCAGCGACTCAGCCTTT TGTAATTAATTGCGATTTGGCTGGGCCGGAATT Antisense, AATTCCGGCCCAGCCAAATCGCAATTAATTACAAAAGGCTGAGTCGCTGCATCTGACTGACATGACTTACA TTGTAACTCTTAAGCAGCCCTATAGTGAGTCGTATTA
EAV pseudoknot OR4	Sense, TAATACGACTCACTATAGGGCGCCTCACGACGGGCCGTAAGACGTGGATATTCTCCTGTGTGGCGTCATGTTGAAG TAGTTATTAGCCACCCAGGAACC Antisense, GGTTCCTGGGTGGCTAATAACTACTTCAACATGACGCCACACAGGAGAATATCCACGTCTTACGGCCCGTC GTGAGGCGCCCTATAGTGAGTCGTATTA
EAV pseudoknot OR5	Sense, TAATACGACTCACTATAGGGCGCCTCCAGCAGGGCCGTAAGACGTGGATATTCTCCTGTGTGGCGTCAGTTGTAA GTAGTTATTAGCCACCCAGGAACC Antisense, GGTTCCTGGGTGGCTAATAACTACTTACAACTGACGCCACACAGGAGAATATCCACGTCTTACGGCCCTGCT GGAGGCGCCCTATAGTGAGTCGTATTA
EAV pseudoknot OR45	Sense, TAATACGACTCACTATAGGGCGCCTCACGACGGGCCGTAAGACGTGGATATTCTCCTGTGTGGCGTCAGTTGTAAG TAGTTATTAGCCACCCAGGAACC Antisense, GGTTCCTGGGTGGCTAATAACTACTTACAACTGACGCCACACAGGAGAATATCCACGTCTTACGGCCCGTCGT GAGGCGCCCTATAGTGAGTCGTATTA
EAV pseudoknot SW4	Sense, TAATACGACTCACTATAGGGCGCCTCTGTTGGGGCCGTAAGACGTGGATATTCTCCTGTGTGGCGTCATGTTGAA GTAGTTATTAGCCACCCAGGAACC Antisense, GGTTCCTGGGTGGCTAATAACTACTTCAACATGACGCCACACAGGAGAATATCCACGTCTTACGGCCCCAAC AGAGGCGCCCTATAGTGAGTCGTATTA
EAV pseudoknot SW5	Sense, TAATACGACTCACTATAGGGCGCCTCCAGCAGGGCCGTAAGACGTGGATATTCTCCTGTGTGGCGTCACAGC AAAGTAGTTATTAGCCACCCAGGAACC Antisense, GGTTCCTGGGTGGCTAATAACTACTTTGCTGTGACGCCACACAGGAGAATATCCACGTCTTACGGCCCTGCTGG AGGCGCCCTATAGTGAGTCGTATTA
EAV pseudoknot SW45	Sense, TAATACGACTCACTATAGGGCGCCTCTGTTGGGGCCGTAAGACGTGGATATTCTCCTGTGTGGCGTCACAGCAAAGT AGTTATTAGCCACCCAGGAACC Antisense, GGTTCCTGGGTGGCTAATAACTACTTTGCTGTGACGCCACACAGGAGAATATCCACGTCTTACGGCCCCAACAG AGGCGCCCTATAGTGAGTCGTATTA

[a]The first two nucleotides of the antisense 5′ termini were modified with 2-*O*-Me (2′-*O*-methyl).

200 10/300 GL column (GE Healthcare) as a control. In order to estimate the molecular size of the protein and RNA complex, the column was calibrated according to the manual (Bio-Rad).

Statistical analysis. All experiments were performed with at least three independent replicates. Data were analyzed using GraphPad Prism software (GraphPad) and are presented as means ± standard errors of the means (SEM). Statistical analyses were performed using unpaired Student's *t* test. A *P* value of less than 0.05 was considered statistically significant.

ACKNOWLEDGMENTS

We thank Wen-Hai Feng (China Agricultural University) for his helpful suggestions and critical reviews of the manuscript and Takashi Fujita (Institute for Virus Research, Kyoto University, Tokyo, Japan) for kindly providing pEF-BOS plasmids.

This work was supported by the Key Project of National Natural Science Funds (31490601) and National Natural Science Funds (31502043).

REFERENCES

1. Janeway CA, Jr, Medzhitov R. 2002. Innate immune recognition. Annu Rev Immunol 20:197–216. https://doi.org/10.1146/annurev.immunol.20.083001.084359.
2. Medzhitov R, Janeway C, Jr. 2000. Innate immune recognition: mechanisms and pathways. Immunol Rev 173:89–97. https://doi.org/10.1034/j.1600-065X.2000.917309.x.

3. Takaoka A, Yanai H. 2006. Interferon signalling network in innate defence. Cell Microbiol 8:907–922. https://doi.org/10.1111/j.1462-5822.2006.00716.x.
4. Hornung V, Guenthner-Biller M, Bourquin C, Ablasser A, Schlee M, Uematsu S, Noronha A, Manoharan M, Akira S, de Fougerolles A, Endres S, Hartmann G. 2005. Sequence-specific potent induction of IFN-alpha by short interfering RNA in plasmacytoid dendritic cells through TLR7. Nat Med 11:263–270. https://doi.org/10.1038/nm1191.
5. Matsumoto M, Funami K, Tanabe M, Oshiumi H, Shingai M, Seto Y, Yamamoto A, Seya T. 2003. Subcellular localization of toll-like receptor 3 in human dendritic cells. J Immunol 171:3154–3162. https://doi.org/10.4049/jimmunol.171.6.3154.
6. Alexopoulou L, Holt AC, Medzhitov R, Flavell RA. 2001. Recognition of double-stranded RNA and activation of NF-kappaB by Toll-like receptor 3. Nature 413:732–738. https://doi.org/10.1038/35099560.
7. Diebold SS, Kaisho T, Hemmi H, Akira S, Reis e Sousa C. 2004. Innate antiviral responses by means of TLR7-mediated recognition of single-stranded RNA. Science 303:1529–1531. https://doi.org/10.1126/science.1093616.
8. Heil F, Hemmi H, Hochrein H, Ampenberger F, Kirschning C, Akira S, Lipford G, Wagner H, Bauer S. 2004. Species-specific recognition of single-stranded RNA via toll-like receptor 7 and 8. Science 303:1526–1529. https://doi.org/10.1126/science.1093620.
9. Hemmi H, Takeuchi O, Kawai T, Kaisho T, Sato S, Sanjo H, Matsumoto M, Hoshino K, Wagner H, Takeda K, Akira S. 2000. A Toll-like receptor recognizes bacterial DNA. Nature 408:740–745. https://doi.org/10.1038/35047123.
10. Wu J, Chen ZJ. 2014. Innate immune sensing and signaling of cytosolic nucleic acids. Annu Rev Immunol 32:461–488. https://doi.org/10.1146/annurev-immunol-032713-120156.
11. Yoneyama M, Kikuchi M, Natsukawa T, Shinobu N, Imaizumi T, Miyagishi M, Taira K, Akira S, Fujita T. 2004. The RNA helicase RIG-I has an essential function in double-stranded RNA-induced innate antiviral responses. Nat Immunol 5:730–737. https://doi.org/10.1038/ni1087.
12. Cui S, Eisenacher K, Kirchhofer A, Brzozka K, Lammens A, Lammens K, Fujita T, Conzelmann KK, Krug A, Hopfner KP. 2008. The C-terminal regulatory domain is the RNA 5′-triphosphate sensor of RIG-I. Mol Cell 29:169–179. https://doi.org/10.1016/j.molcel.2007.10.032.
13. Rodriguez KR, Bruns AM, Horvath CM. 2014. MDA5 and LGP2: accomplices and antagonists of antiviral signal transduction. J Virol 88:8194–8200. https://doi.org/10.1128/JVI.00640-14.
14. Ahmad S, Hur S. 2015. Helicases in antiviral immunity: dual properties as sensors and effectors. Trends Biochem Sci 40:576–585. https://doi.org/10.1016/j.tibs.2015.08.001.
15. Takeuchi O, Akira S. 2009. Innate immunity to virus infection. Immunol Rev 227:75–86. https://doi.org/10.1111/j.1600-065X.2008.00737.x.
16. El Maadidi S, Faletti L, Berg B, Wenzl C, Wieland K, Chen ZJ, Maurer U, Borner C. 2014. A novel mitochondrial MAVS/caspase-8 platform links RNA virus-induced innate antiviral signaling to Bax/Bak-independent apoptosis. J Immunol 192:1171–1183. https://doi.org/10.4049/jimmunol.1300842.
17. Sadler AJ, Williams BR. 2008. Interferon-inducible antiviral effectors. Nat Rev Immunol 8:559–568. https://doi.org/10.1038/nri2314.
18. George CX, John L, Samuel CE. 2014. An RNA editor, adenosine deaminase acting on double-stranded RNA (ADAR1). J Interferon Cytokine Res 34:437–446. https://doi.org/10.1089/jir.2014.0001.
19. Kato H, Takeuchi O, Sato S, Yoneyama M, Yamamoto M, Matsui K, Uematsu S, Jung A, Kawai T, Ishii KJ, Yamaguchi O, Otsu K, Tsujimura T, Koh CS, Reis e Sousa C, Matsuura Y, Fujita T, Akira S. 2006. Differential roles of MDA5 and RIG-I helicases in the recognition of RNA viruses. Nature 441:101–105. https://doi.org/10.1038/nature04734.
20. Yoneyama M, Fujita T. 2010. Recognition of viral nucleic acids in innate immunity. Rev Med Virol 20:4–22. https://doi.org/10.1002/rmv.633.
21. Rehwinkel J, Reis e Sousa C. 2010. RIGorous detection: exposing virus through RNA sensing. Science 327:284–286. https://doi.org/10.1126/science.1185068.
22. Saito T, Owen DM, Jiang F, Marcotrigiano J, Gale M, Jr. 2008. Innate immunity induced by composition-dependent RIG-I recognition of hepatitis C virus RNA. Nature 454:523–527. https://doi.org/10.1038/nature07106.
23. Andrejeva J, Childs KS, Young DF, Carlos TS, Stock N, Goodbourn S, Randall RE. 2004. The V proteins of paramyxoviruses bind the IFN-inducible RNA helicase, mda-5, and inhibit its activation of the IFN-beta promoter. Proc Natl Acad Sci U S A 101:17264–17269. https://doi.org/10.1073/pnas.0407639101.
24. Benitez AA, Panis M, Xue J, Varble A, Shim JV, Frick AL, Lopez CB, Sachs D, tenOever BR. 2015. In vivo RNAi screening identifies MDA5 as a significant contributor to the cellular defense against influenza A virus. Cell Rep 11:1714–1726. https://doi.org/10.1016/j.celrep.2015.05.032.
25. Strahle L, Garcin D, Kolakofsky D. 2006. Sendai virus defective-interfering genomes and the activation of interferon-beta. Virology 351:101–111. https://doi.org/10.1016/j.virol.2006.03.022.
26. Zhang X, Wang C, Schook LB, Hawken RJ, Rutherford MS. 2000. An RNA helicase, RHIV-1, induced by porcine reproductive and respiratory syndrome virus (PRRSV) is mapped on porcine chromosome 10q13. Microb Pathog 28:267–278. https://doi.org/10.1006/mpat.1999.0349.
27. Luthra P, Sun D, Silverman RH, He B. 2011. Activation of IFN-β expression by a viral mRNA through RNase L and MDA5. Proc Natl Acad Sci U S A 108:2118–2123. https://doi.org/10.1073/pnas.1012409108.
28. Runge S, Sparrer KM, Lassig C, Hembach K, Baum A, Garcia-Sastre A, Soding J, Conzelmann KK, Hopfner KP. 2014. In vivo ligands of MDA5 and RIG-I in measles virus-infected cells. PLoS Pathog 10:e1004081. https://doi.org/10.1371/journal.ppat.1004081.
29. Loo YM, Fornek J, Crochet N, Bajwa G, Perwitasari O, Martinez-Sobrido L, Akira S, Gill MA, Garcia-Sastre A, Katze MG, Gale M, Jr. 2008. Distinct RIG-I and MDA5 signaling by RNA viruses in innate immunity. J Virol 82:335–345. https://doi.org/10.1128/JVI.01080-07.
30. Fredericksen BL, Keller BC, Fornek J, Katze MG, Gale M, Jr. 2008. Establishment and maintenance of the innate antiviral response to West Nile virus involves both RIG-I and MDA5 signaling through IPS-1. J Virol 82:609–616. https://doi.org/10.1128/JVI.01305-07.
31. Sumpter R, Jr, Loo YM, Foy E, Li K, Yoneyama M, Fujita T, Lemon SM, Gale M, Jr. 2005. Regulating intracellular antiviral defense and permissiveness to hepatitis C virus RNA replication through a cellular RNA helicase, RIG-I. J Virol 79:2689–2699. https://doi.org/10.1128/JVI.79.5.2689-2699.2005.
32. Weber F, Wagner V, Rasmussen SB, Hartmann R, Paludan SR. 2006. Double-stranded RNA is produced by positive-strand RNA viruses and DNA viruses but not in detectable amounts by negative-strand RNA viruses. J Virol 80:5059–5064. https://doi.org/10.1128/JVI.80.10.5059-5064.2006.
33. Liu G, Park HS, Pyo HM, Liu Q, Zhou Y. 2015. Influenza A virus panhandle structure is directly involved in RIG-I activation and interferon induction. J Virol 89:6067–6079. https://doi.org/10.1128/JVI.00232-15.
34. Hornung V, Ellegast J, Kim S, Brzozka K, Jung A, Kato H, Poeck H, Akira S, Conzelmann KK, Schlee M, Endres S, Hartmann G. 2006. 5′-Triphosphate RNA is the ligand for RIG-I. Science 314:994–997. https://doi.org/10.1126/science.1132505.
35. Pichlmair A, Schulz O, Tan CP, Naslund TI, Liljestrom P, Weber F, Reis e Sousa C. 2006. RIG-I-mediated antiviral responses to single-stranded RNA bearing 5′-phosphates. Science 314:997–1001. https://doi.org/10.1126/science.1132998.
36. Schlee M, Roth A, Hornung V, Hagmann CA, Wimmenauer V, Barchet W, Coch C, Janke M, Mihailovic A, Wardle G, Juranek S, Kato H, Kawai T, Poeck H, Fitzgerald KA, Takeuchi O, Akira S, Tuschl T, Latz E, Ludwig J, Hartmann G. 2009. Recognition of 5′ triphosphate by RIG-I helicase requires short blunt double-stranded RNA as contained in panhandle of negative-strand virus. Immunity 31:25–34. https://doi.org/10.1016/j.immuni.2009.05.008.
37. Fujita T. 2009. A nonself RNA pattern: tri-p to panhandle. Immunity 31:4–5. https://doi.org/10.1016/j.immuni.2009.06.014.
38. Goubau D, Schlee M, Deddouche S, Pruijssers AJ, Zillinger T, Goldeck M, Schuberth C, Van der Veen AG, Fujimura T, Rehwinkel J, Iskarpatyoti JA, Barchet W, Ludwig J, Dermody TS, Hartmann G, Reis ESC. 2014. Antiviral immunity via RIG-I-mediated recognition of RNA bearing 5′-diphosphates. Nature 514:372–375. https://doi.org/10.1038/nature13590.
39. Kato H, Sato S, Yoneyama M, Yamamoto M, Uematsu S, Matsui K, Tsujimura T, Takeda K, Fujita T, Takeuchi O, Akira S. 2005. Cell type-specific involvement of RIG-I in antiviral response. Immunity 23:19–28. https://doi.org/10.1016/j.immuni.2005.04.010.
40. Kuhn JH, Lauck M, Bailey AL, Shchetinin AM, Vishnevskaya TV, Bao Y, Ng TF, LeBreton M, Schneider BS, Gillis A, Tamoufe U, Diffo Jle D, Takuo JM, Kondov NO, Coffey LL, Wolfe ND, Delwart E, Clawson AN, Postnikova E, Bollinger L, Lackemeyer MG, Radoshitzky SR, Palacios G, Wada J, Shevtsova ZV, Jahrling PB, Lapin BA, Deriabin PG, Dunowska M, Alkhovsky SV, Rogers J, Friedrich TC, O'Connor DH, Goldberg TL. 2016. Reorganization and expansion of the nidoviral family Arteriviridae. Arch Virol 161:755–768. https://doi.org/10.1007/s00705-015-2672-z.

41. Cavanagh D. 1997. Nidovirales a new order comprising Coronaviridae and Arteriviridae. Arch Virol 142:629–633.
42. Thiel HJ, Meyers G, Stark R, Tautz N, Rumenapf T, Unger G, Conzelmann KK. 1993. Molecular characterization of positive-strand RNA viruses pestiviruses and the porcine reproductive and respiratory syndrome virus (PRRSV). Arch Virol Suppl 7:41–52. https://doi.org/10.1007/978-3-7091-9300-6_4.
43. Van Reeth K, Labarque G, Nauwynck H, Pensaert M. 1999. Differential production of proinflammatory cytokines in the pig lung during different respiratory virus infections: correlations with pathogenicity. Res Vet Sci 67:47–52. https://doi.org/10.1053/rvsc.1998.0277.
44. Lee SM, Schommer SK, Kleiboeker SB. 2004. Porcine reproductive and respiratory syndrome virus field isolates differ in in vitro interferon phenotypes. Vet Immunol Immunopathol 102:217–231. https://doi.org/10.1016/j.vetimm.2004.09.009.
45. Albina E, Carrat C, Charley B. 1998. Interferon-alpha response to swine arterivirus (PoAV), the porcine reproductive and respiratory syndrome virus. J Interferon Cytokine Res 18:485–490. https://doi.org/10.1089/jir.1998.18.485.
46. Brockmeier SL, Lager KM, Grubman MJ, Brough DE, Ettyreddy D, Sacco RE, Gauger PC, Loving CL, Vorwald AC, Kehrli ME, Jr, Lehmkuhl HD. 2009. Adenovirus-mediated expression of interferon-alpha delays viral replication and reduces disease signs in swine challenged with porcine reproductive and respiratory syndrome virus. Viral Immunol 22:173–180. https://doi.org/10.1089/vim.2008.0075.
47. Loving CL, Brockmeier SL, Sacco RE. 2007. Differential type I interferon activation and susceptibility of dendritic cell populations to porcine arterivirus. Immunology 120:217–229. https://doi.org/10.1111/j.1365-2567.2006.02493.x.
48. Genini S, Delputte PL, Malinverni R, Cecere M, Stella A, Nauwynck HJ, Giuffra E. 2008. Genome-wide transcriptional response of primary alveolar macrophages following infection with porcine reproductive and respiratory syndrome virus. J Gen Virol 89:2550–2564. https://doi.org/10.1099/vir.0.2008/003244-0.
49. Snijder EJ, Kikkert M, Fang Y. 2013. Arterivirus molecular biology and pathogenesis. J Gen Virol 94:2141–2163. https://doi.org/10.1099/vir.0.056341-0.
50. Hart OM, Athie-Morales V, O'Connor GM, Gardiner CM. 2005. TLR7/8-mediated activation of human NK cells results in accessory cell-dependent IFN-gamma production. J Immunol 175:1636–1642. https://doi.org/10.4049/jimmunol.175.3.1636.
51. Zhou Y, Guo M, Wang X, Li J, Wang Y, Ye L, Dai M, Zhou L, Persidsky Y, Ho W. 2013. TLR3 activation efficiency by high or low molecular mass poly I:C. Innate Immun 19:184–192. https://doi.org/10.1177/1753425912459975.
52. Kao C, Zheng M, Rudisser S. 1999. A simple and efficient method to reduce nontemplated nucleotide addition at the 3 terminus of RNAs transcribed by T7 RNA polymerase. RNA 5:1268–1272. https://doi.org/10.1017/S1355838299991033.
53. Milligan JF, Groebe DR, Witherell GW, Uhlenbeck OC. 1987. Oligoribonucleotide synthesis using T7 RNA polymerase and synthetic DNA templates. Nucleic Acids Res 15:8783–8798. https://doi.org/10.1093/nar/15.21.8783.
54. Sato S, Li K, Kameyama T, Hayashi T, Ishida Y, Murakami S, Watanabe T, Iijima S, Sakurai Y, Watashi K, Tsutsumi S, Sato Y, Akita H, Wakita T, Rice CM, Harashima H, Kohara M, Tanaka Y, Takaoka A. 2015. The RNA sensor RIG-I dually functions as an innate sensor and direct antiviral factor for hepatitis B virus. Immunity 42:123–132. https://doi.org/10.1016/j.immuni.2014.12.016.
55. Zuker M. 2003. Mfold web server for nucleic acid folding and hybridization prediction. Nucleic Acids Res 31:3406–3415. https://doi.org/10.1093/nar/gkg595.
56. Borer PN, Dengler B, Tinoco I, Jr, Uhlenbeck OC. 1974. Stability of ribonucleic acid double-stranded helices. J Mol Biol 86:843–853. https://doi.org/10.1016/0022-2836(74)90357-X.
57. Tinoco I, Jr, Uhlenbeck OC, Levine MD. 1971. Estimation of secondary structure in ribonucleic acids. Nature 230:362–367. https://doi.org/10.1038/230362a0.
58. Beerens N, Snijder EJ. 2007. An RNA pseudoknot in the 3′ end of the arterivirus genome has a critical role in regulating viral RNA synthesis. J Virol 81:9426–9436. https://doi.org/10.1128/JVI.00747-07.
59. Goebel SJ, Hsue B, Dombrowski TF, Masters PS. 2004. Characterization of the RNA components of a putative molecular switch in the 3′ untranslated region of the murine coronavirus genome. J Virol 78:669–682. https://doi.org/10.1128/JVI.78.2.669-682.2004.
60. Choi YJ, Yun SI, Kang SY, Lee YM. 2006. Identification of 5′ and 3′ cis-acting elements of the porcine reproductive and respiratory syndrome virus: acquisition of novel 5′ AU-rich sequences restored replication of a 5′-proximal 7-nucleotide deletion mutant. J Virol 80:723–736. https://doi.org/10.1128/JVI.80.2.723-736.2006.
61. Beerens N, Snijder EJ. 2006. RNA signals in the 3′ terminus of the genome of equine arteritis virus are required for viral RNA synthesis. J Gen Virol 87:1977–1983. https://doi.org/10.1099/vir.0.81750-0.
62. Lai MM, Brayton PR, Armen RC, Patton CD, Pugh C, Stohlman SA. 1981. Mouse hepatitis virus A59: mRNA structure and genetic localization of the sequence divergence from hepatotropic strain MHV-3. J Virol 39:823–834.
63. Leung DW, Amarasinghe GK. 2016. When your cap matters: structural insights into self vs non-self recognition of 5′ RNA by immunomodulatory host proteins. Curr Opin Struct Biol 36:133–141. https://doi.org/10.1016/j.sbi.2016.02.001.
64. Li Y, Treffers EE, Napthine S, Tas A, Zhu L, Sun Z, Bell S, Mark BL, van Veelen PA, van Hemert MJ, Firth AE, Brierley I, Snijder EJ, Fang Y. 2014. Transactivation of programmed ribosomal frameshifting by a viral protein. Proc Natl Acad Sci U S A 111:E2172–E2181. https://doi.org/10.1073/pnas.1321930111.
65. Baric RS, Stohlman SA, Lai MM. 1983. Characterization of replicative intermediate RNA of mouse hepatitis virus: presence of leader RNA sequences on nascent chains. J Virol 48:633–640.
66. Kuo LL, Harty JT, Erickson L, Palmer GA, Plagemann PG. 1991. A nested set of eight RNAs is formed in macrophages infected with lactate dehydrogenase-elevating virus. J Virol 65:5118–5123.
67. Meng XJ, Paul PS, Morozov I, Halbur PG. 1996. A nested set of six or seven subgenomic mRNAs is formed in cells infected with different isolates of porcine reproductive and respiratory syndrome virus. J Gen Virol 77(Part 6):1265–1270. https://doi.org/10.1099/0022-1317-77-6-1265.
68. Sun Z, Liu C, Tan F, Gao F, Liu P, Qin A, Yuan S. 2010. Identification of dispensable nucleotide sequence in 3′ untranslated region of porcine reproductive and respiratory syndrome virus. Virus Res 154:38–47. https://doi.org/10.1016/j.virusres.2010.08.027.
69. Williams GD, Chang RY, Brian DA. 1999. A phylogenetically conserved hairpin-type 3′ untranslated region pseudoknot functions in coronavirus RNA replication. J Virol 73:8349–8355.
70. Wyatt JR, Puglisi JD, Tinoco I, Jr. 1990. RNA pseudoknots. Stability and loop size requirements. J Mol Biol 214:455–470.
71. Patel D, Nan Y, Shen M, Ritthipichai K, Zhu X, Zhang YJ. 2010. Porcine reproductive and respiratory syndrome virus inhibits type I interferon signaling by blocking STAT1/STAT2 nuclear translocation. J Virol 84:11045–11055. https://doi.org/10.1128/JVI.00655-10.
72. Wang R, Nan Y, Yu Y, Zhang YJ. 2013. Porcine reproductive and respiratory syndrome virus Nsp1beta inhibits interferon-activated JAK/STAT signal transduction by inducing karyopherin-alpha1 degradation. J Virol 87:5219–5228. https://doi.org/10.1128/JVI.02643-12.
73. Buddaert W, Van Reeth K, Pensaert M. 1998. In vivo and in vitro interferon (IFN) studies with the porcine reproductive and respiratory syndrome virus (PRRSV). Adv Exp Med Biol 440:461–467. https://doi.org/10.1007/978-1-4615-5331-1_59.
74. Chen Z, Lawson S, Sun Z, Zhou X, Guan X, Christopher-Hennings J, Nelson EA, Fang Y. 2010. Identification of two auto-cleavage products of nonstructural protein 1 (nsp1) in porcine reproductive and respiratory syndrome virus infected cells: nsp1 function as interferon antagonist. Virology 398:87–97. https://doi.org/10.1016/j.virol.2009.11.033.
75. Luo R, Xiao S, Jiang Y, Jin H, Wang D, Liu M, Chen H, Fang L. 2008. Porcine reproductive and respiratory syndrome virus (PRRSV) suppresses interferon-beta production by interfering with the RIG-I signaling pathway. Mol Immunol 45:2839–2846. https://doi.org/10.1016/j.molimm.2008.01.028.
76. Kim O, Sun Y, Lai FW, Song C, Yoo D. 2010. Modulation of type I interferon induction by porcine reproductive and respiratory syndrome virus and degradation of CREB-binding protein by non-structural protein 1 in MARC-145 and HeLa cells. Virology 402:315–326. https://doi.org/10.1016/j.virol.2010.03.039.
77. Huang C, Zhang Q, Guo XK, Yu ZB, Xu AT, Tang J, Feng WH. 2014. Porcine reproductive and respiratory syndrome virus nonstructural protein 4 antagonizes beta interferon expression by targeting the NF-kappaB essential modulator. J Virol 88:10934–10945. https://doi.org/10.1128/JVI.01396-14.
78. Overend C, Mitchell R, He D, Rompato G, Grubman MJ, Garmendia AE. 2007. Recombinant swine beta interferon protects swine alveolar mac-

rophages and MARC-145 cells from infection with porcine reproductive and respiratory syndrome virus. J Gen Virol 88:925–931. https://doi.org/10.1099/vir.0.82585-0.
79. Chang HW, Jeng CR, Liu JJ, Lin TL, Chang CC, Chia MY, Tsai YC, Pang VF. 2005. Reduction of porcine reproductive and respiratory syndrome virus (PRRSV) infection in swine alveolar macrophages by porcine circovirus 2 (PCV2)-induced interferon-alpha. Vet Microbiol 108:167–177. https://doi.org/10.1016/j.vetmic.2005.03.010.
80. Verheije MH, Olsthoorn RCL, Kroese MV, Rottier PJM, Meulenberg JJM. 2002. Kissing interaction between 3′ noncoding and coding sequences is essential for porcine arterivirus RNA replication. J Virol 76:1521–1526. https://doi.org/10.1128/JVI.76.3.1521-1526.2002.
81. Lu C, Xu H, Ranjith-Kumar CT, Brooks MT, Hou TY, Hu F, Herr AB, Strong RK, Kao CC, Li P. 2010. The structural basis of 5′ triphosphate double-stranded RNA recognition by RIG-I C-terminal domain. Structure 18:1032–1043. https://doi.org/10.1016/j.str.2010.05.007.
82. Kato H, Takeuchi O, Mikamo-Satoh E, Hirai R, Kawai T, Matsushita K, Hiiragi A, Dermody TS, Fujita T, Akira S. 2008. Length-dependent recognition of double-stranded ribonucleic acids by retinoic acid-inducible gene-I and melanoma differentiation-associated gene 5. J Exp Med 205:1601–1610. https://doi.org/10.1084/jem.20080091.
83. Kato H, Takeuchi O, Akira S. 2006. Cell type specific involvement of RIG-I in antiviral responses. Nihon Rinsho 64:1244–1247.
84. van Kasteren PB, Beugeling C, Ninaber DK, Frias-Staheli N, van Boheemen S, Garcia-Sastre A, Snijder EJ, Kikkert M. 2012. Arterivirus and nairovirus ovarian tumor domain-containing deubiquitinases target activated RIG-I to control innate immune signaling. J Virol 86:773–785. https://doi.org/10.1128/JVI.06277-11.
85. Wang Y, Ludwig J, Schuberth C, Goldeck M, Schlee M, Li H, Juranek S, Sheng G, Micura R, Tuschl T, Hartmann G, Patel DJ. 2010. Structural and functional insights into 5′-ppp RNA pattern recognition by the innate immune receptor RIG-I. Nat Struct Mol Biol 17:781–787. https://doi.org/10.1038/nsmb.1863.
86. Devarkar SC, Wang C, Miller MT, Ramanathan A, Jiang F, Khan AG, Patel SS, Marcotrigiano J. 2016. Structural basis for m7G recognition and 2′-O-methyl discrimination in capped RNAs by the innate immune receptor RIG-I. Proc Natl Acad Sci U S A 113:596–601. https://doi.org/10.1073/pnas.1515152113.
87. Furuichi Y, Shatkin AJ. 2000. Viral and cellular mRNA capping: past and prospects. Adv Virus Res 55:135–184. https://doi.org/10.1016/S0065-3527(00)55003-9.
88. Lehmann KC, Hooghiemstra L, Gulyaeva A, Samborskiy DV, Zevenhoven-Dobbe JC, Snijder EJ, Gorbalenya AE, Posthuma CC. 2015. Arterivirus nsp12 versus the coronavirus nsp16 2′-O-methyltransferase: comparison of the C-terminal cleavage products of two nidovirus pp1ab polyproteins. J Gen Virol 96:2643–2655. https://doi.org/10.1099/vir.0.000209.
89. Weingartl HM, Sabara M, Pasick J, van Moorlehem E, Babiuk L. 2002. Continuous porcine cell lines developed from alveolar macrophages: partial characterization and virus susceptibility. J Virol Methods 104:203–216. https://doi.org/10.1016/S0166-0934(02)00085-X.
90. Xiao S, Zhang A, Zhang C, Ni H, Gao J, Wang C, Zhao Q, Wang X, Wang X, Ma C, Liu H, Li N, Mu Y, Sun Y, Zhang G, Hiscox JA, Hsu WH, Zhou E-M. 2014. Heme oxygenase-1 acts as an antiviral factor for porcine reproductive and respiratory syndrome virus infection and over-expression inhibits virus replication in vitro. Antiviral Res 110:60–69. https://doi.org/10.1016/j.antiviral.2014.07.011.
91. Schmittgen TD, Livak KJ. 2008. Analyzing real-time PCR data by the comparative C(T) method. Nat Protoc 3:1101–1108. https://doi.org/10.1038/nprot.2008.73.
92. Chen XX, Quan R, Guo XK, Gao L, Shi J, Feng WH. 2014. Up-regulation of pro-inflammatory factors by HP-PRRSV infection in microglia: implications for HP-PRRSV neuropathogenesis. Vet Microbiol 170:48–57. https://doi.org/10.1016/j.vetmic.2014.01.031.
93. De Rijk P, Wuyts J, De Wachter R. 2003. RnaViz 2: an improved representation of RNA secondary structure. Bioinformatics 19:299–300. https://doi.org/10.1093/bioinformatics/19.2.299.